Regional and global seismic tomography: Imaging the structure and dynamics of the Earth

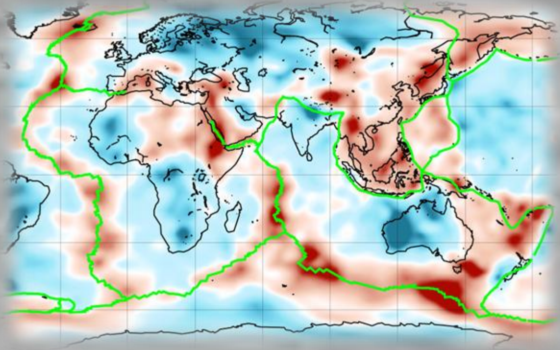

Sergei Lebedev

Dublin Institute for Advanced Studies

Earth structure and dynamics

Earth's spectacular topography:
consequence of movements deep inside the Earth

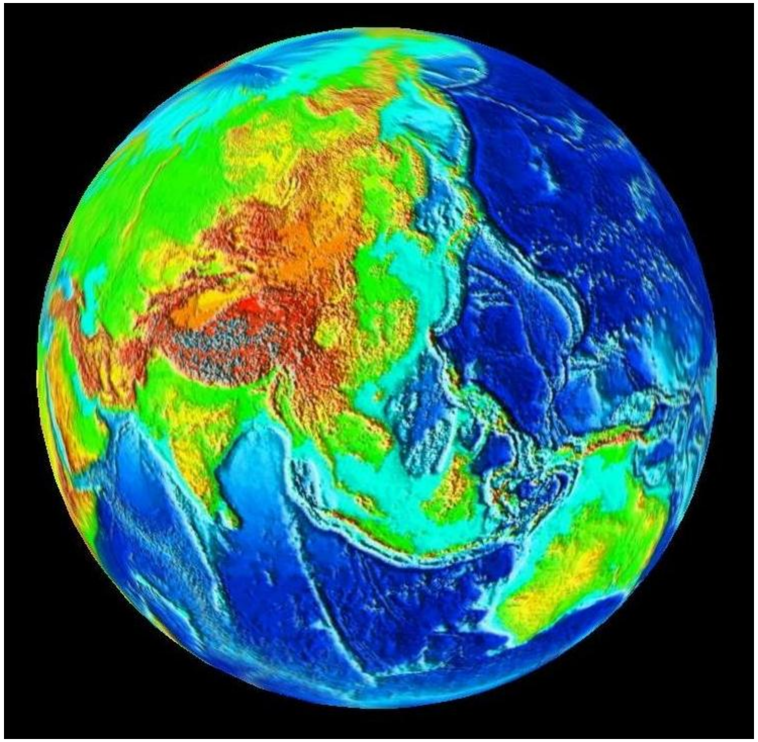

Earth structure and dynamics

What are these movements?

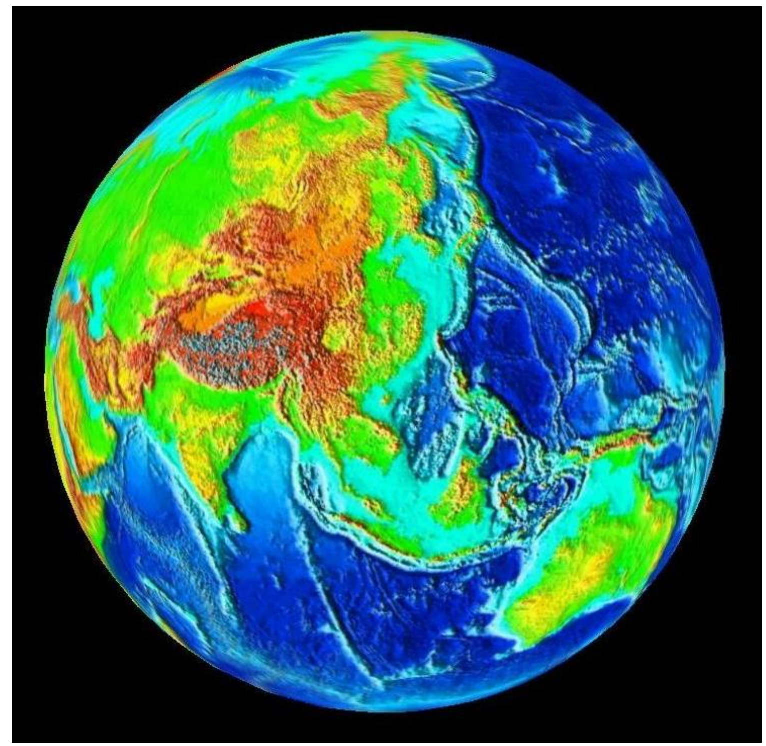

Seismic tomography

Medical imaging

siemens.com

Seismic tomography

Medical imaging

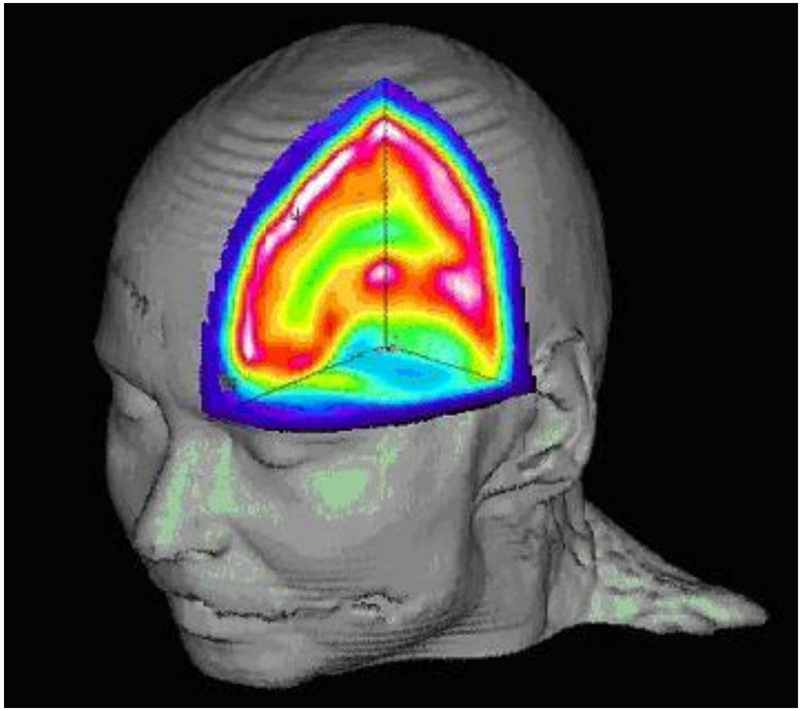

http://particle.uni-wuppertal.de/Schul-Vorlesungen/themen.php

Seismic imaging

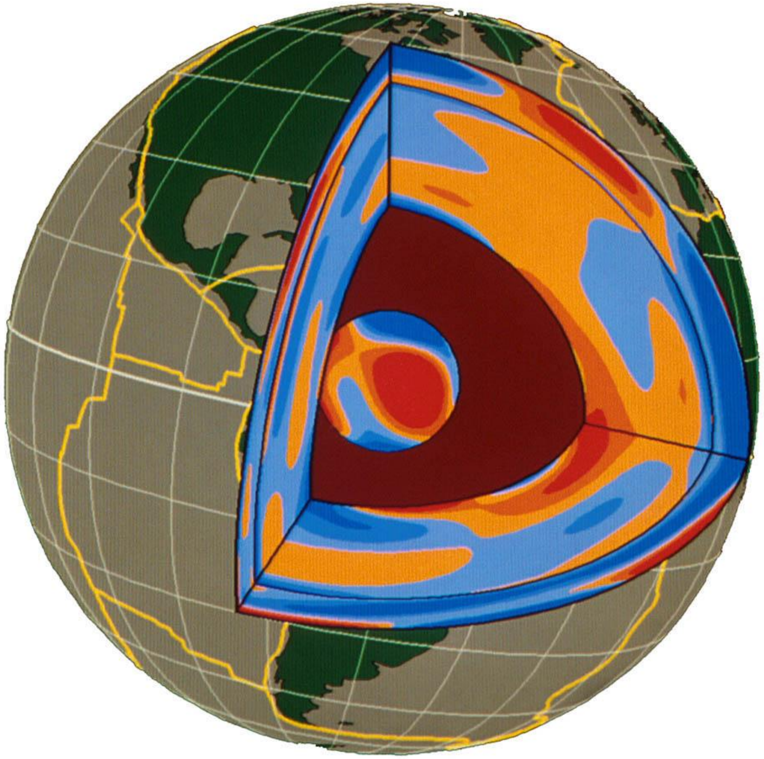

http://www.agu.org/focus_group/SEDI

Seismic tomography

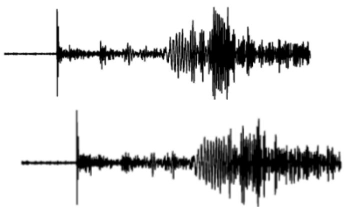

seismograms

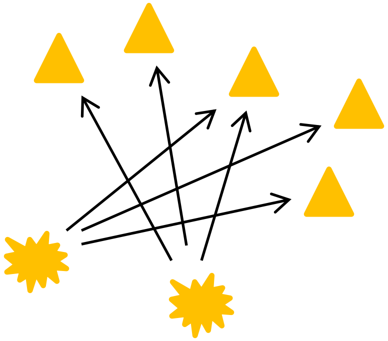

measurements

constrain structure between earthquakes and stations or between stations

- travel-time measurements
- phase-velocity measurements
- waveform inversion

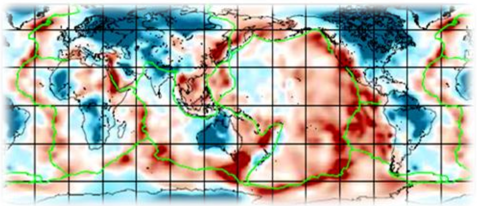

tomographic models

New generation of tomographic models

- Today: explosive growth of seismic networks
- Methodological Advances
- More powerful computers

- More detailed and more accurate models

Global and regional seismic tomography

I. Large-scale tomography:
waveform inversion

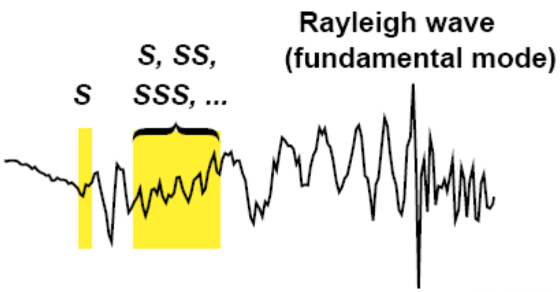

II. Regional tomography:
array imaging

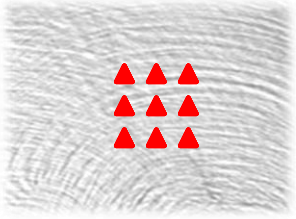

III. Petro-physical inversion

Global and regional seismic tomography

I. Large-scale tomography:
waveform inversion

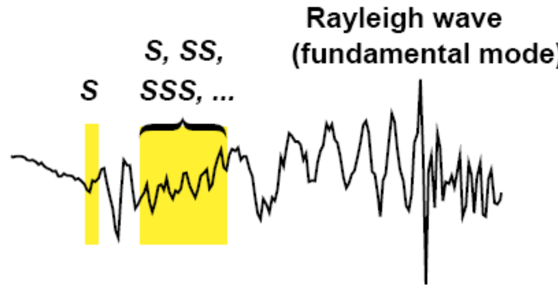

II. Regional tomography:
array imaging

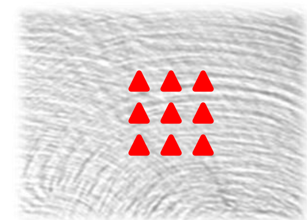

III. Petro-physical inversion

- Global *S*-velocity structure
  and anisotropy

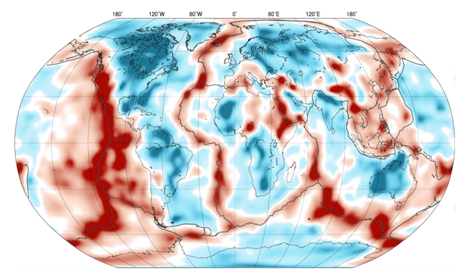

- Lithospheric dynamics
  in the Eastern Mediterranean

- Ireland Array and geothermal applications

I. Waveform Inversion

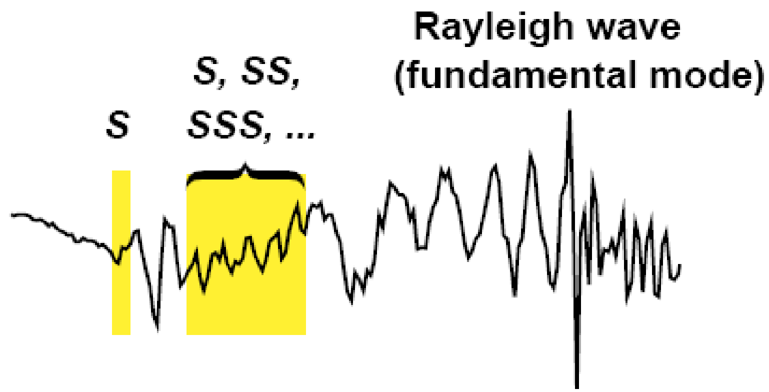

- Constrain Earth structure with full seismic waveforms, not one-per-seismogram observables
- Extract information from the fundamental mode and *S* and multiple *S* waves (interference → individual arrivals often unidentifiable).
- Resolution from near the surface down to ~660-km depth.

Waveform tomography: a timeline

Early 1980s

First applications.

100s of Earth-model parameters adjusted to fit 1000s of seismograms.

Dziewonski & Steim 1982; Woodhouse & Dziewonski 1984.

Late 1980s

Waveform inversions broken into steps.

Extraction of linear equations from one seismogram at a time; solving the resulting linear system for a detailed Earth model.

Cara & Lévêque 1987; Nolet 1990; Gee & Jordan 1992.

Late 1990s

Automated multimode waveform inversions.

Debayle 1999; Lebedev et al. 2005.

Today

Global waveform tomography with O(10**6) seismograms.

Schaeffer & Lebedev 2012.

Automated Multimode Inversion (AMI)

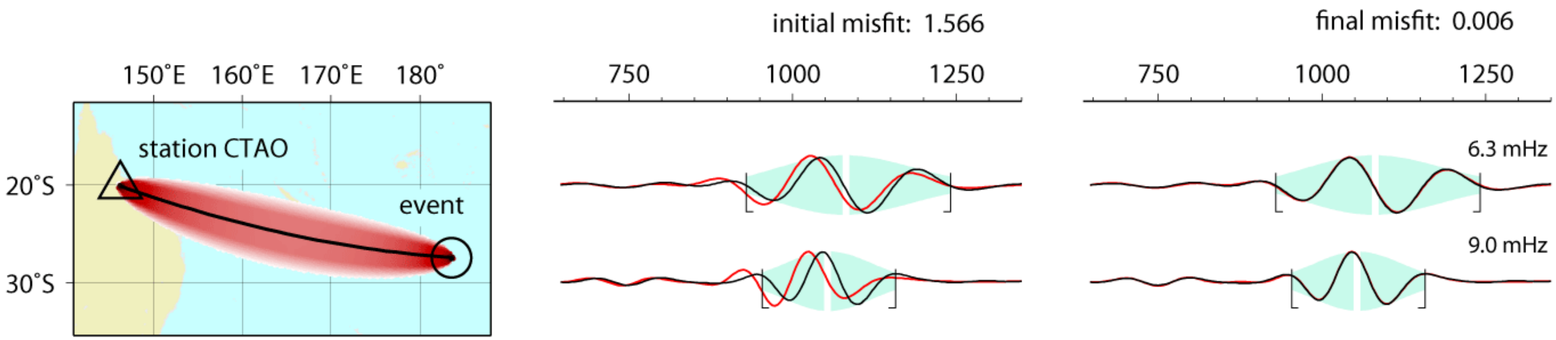

1. Processing very large amounts of data; full automation.

2. Aiming to extract maximum information from each seismogram while ensuring that relevant theoretical approximations hold.

3. Balancing this information when relating it to Earth structure (weighting waves of different amplitudes and different types) so as to constrain unbiased Earth models.

Lebedev 2000; Lebedev & Nolet 2003; Lebedev, Nolet, Meier, van der Hilst (2005)

Automated Multimode Inversion (AMI)

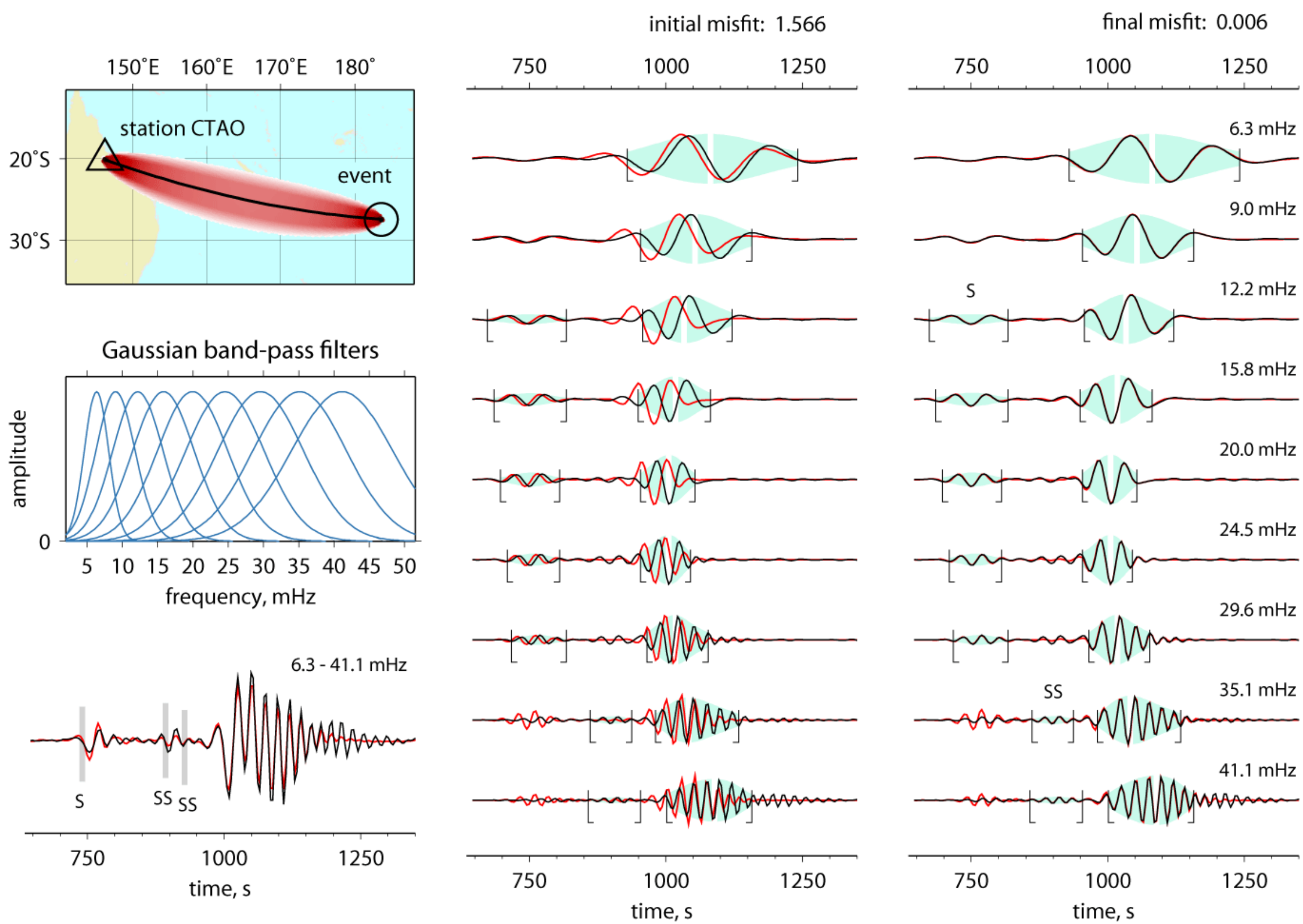

Lebedev 2000; Lebedev & Nolet 2003; Lebedev, Nolet, Meier, van der Hilst (2005)

Automated Multimode Inversion (AMI)

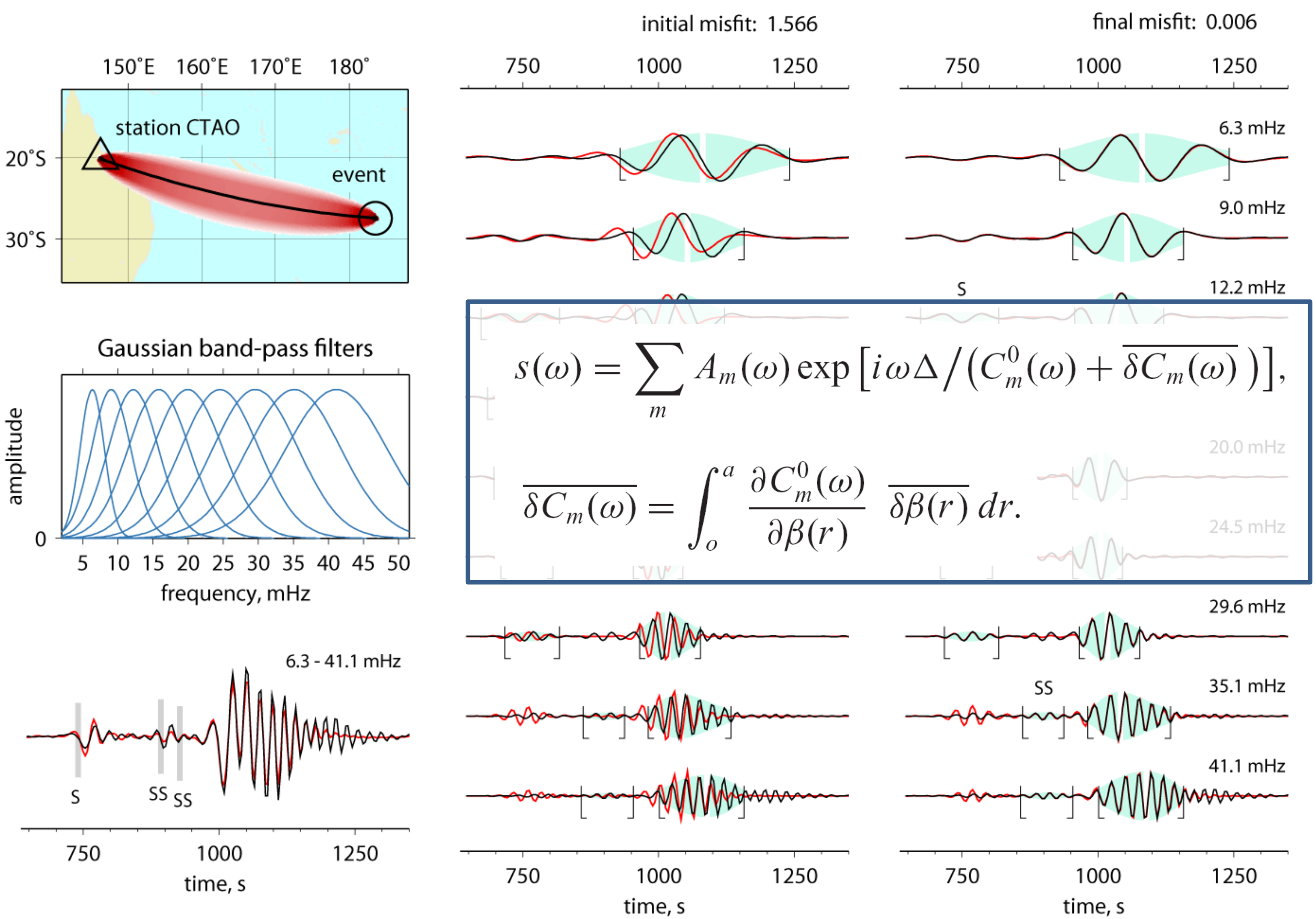

$$s(\omega) = \sum_m A_m(\omega) \exp\left[i\omega\Delta / \left(C_m^0(\omega) + \overline{\delta C_m(\omega)}\right)\right],$$

$$\overline{\delta C_m(\omega)} = \int_o^a \frac{\partial C_m^0(\omega)}{\partial \beta(r)} \, \overline{\delta\beta(r)} \, dr.$$

Lebedev 2000; Lebedev & Nolet 2003; Lebedev, Nolet, Meier, van der Hilst (2005)

Automated Multimode Inversion (AMI)

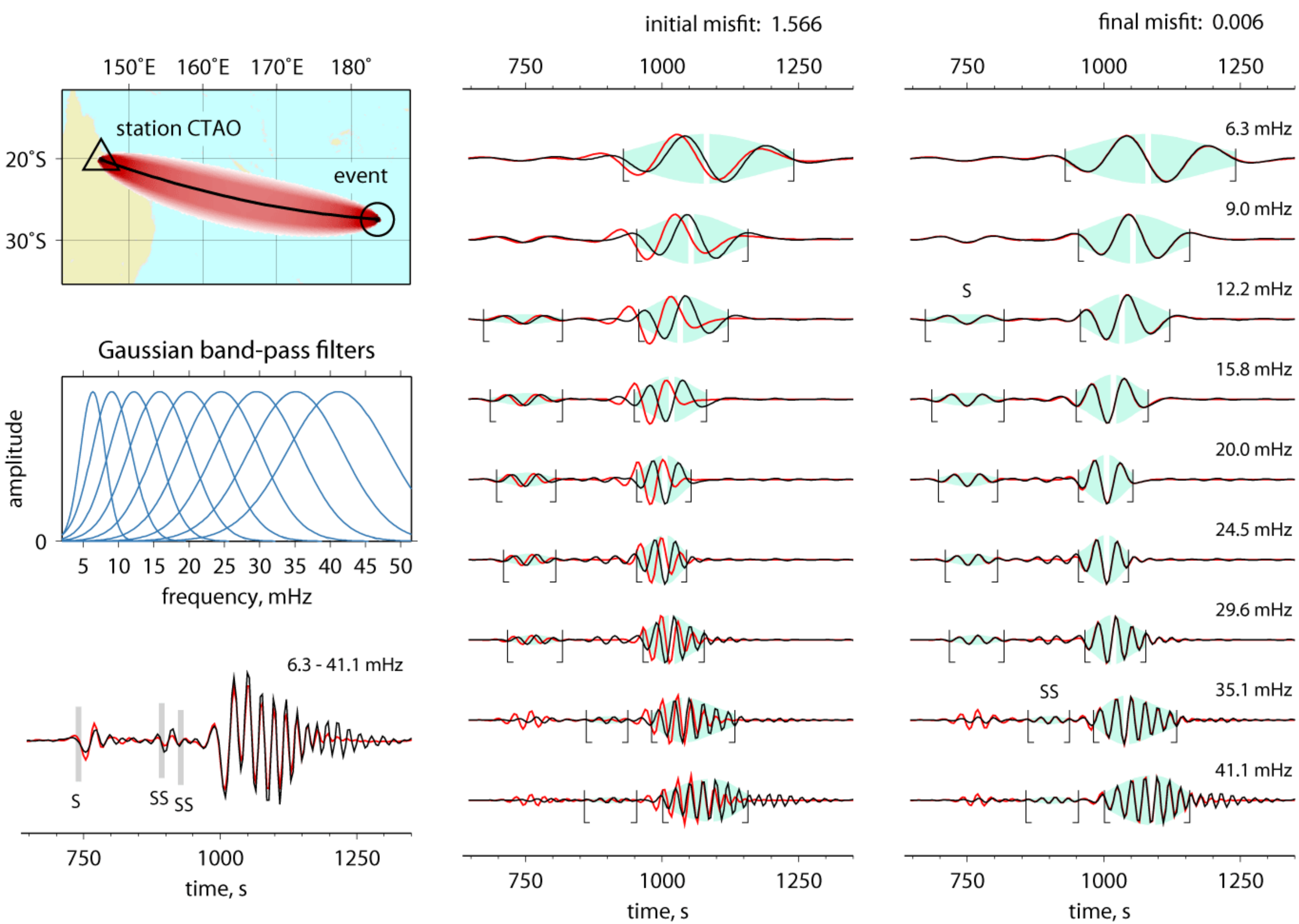

Lebedev 2000; Lebedev & Nolet 2003; Lebedev, Nolet, Meier, van der Hilst (2005)

Tomography Set-up

Three Step Inversion:

1. Automated Multimode Inversion (AMI) of each seismogram
2. Linear Tomographic Inversion
3. Outlier removal

Hybrid 3D Reference Model

Initial crustal model is smoothed Crust2; crustal structure is then inverted for

Mantle velocity: AK135 recomputed at reference period 50s

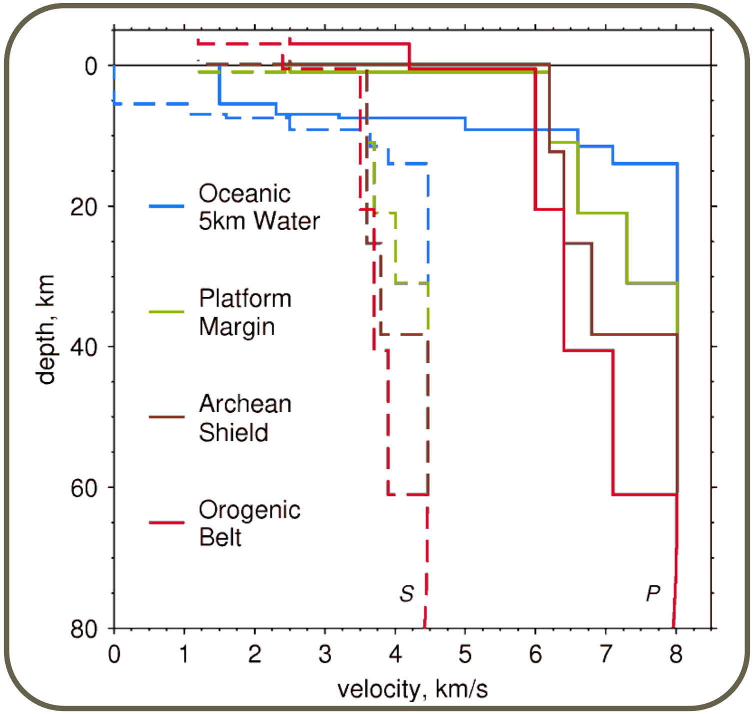

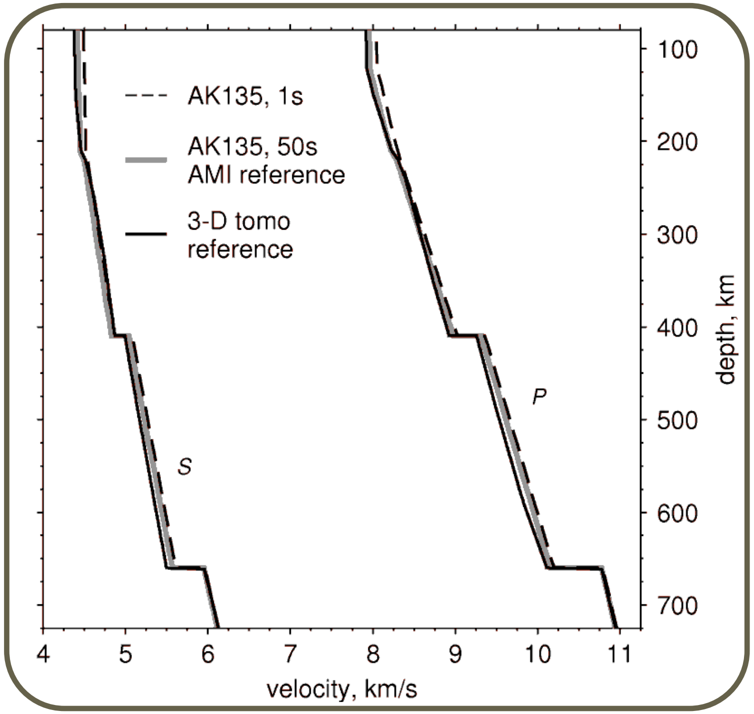

3D Tomographic Inversion

- Linear equations from AMI combined into large system
- 2 co-registered triangular grids (Wang and Dahlen, 1995)
- Sensitivity kernels
- Down-weighting of non-unique paths for more even sampling distribution
- Regularization using lateral smoothing, gradient damping, slight norm damping
- Outlier analysis and removal

Integration and Model Grids

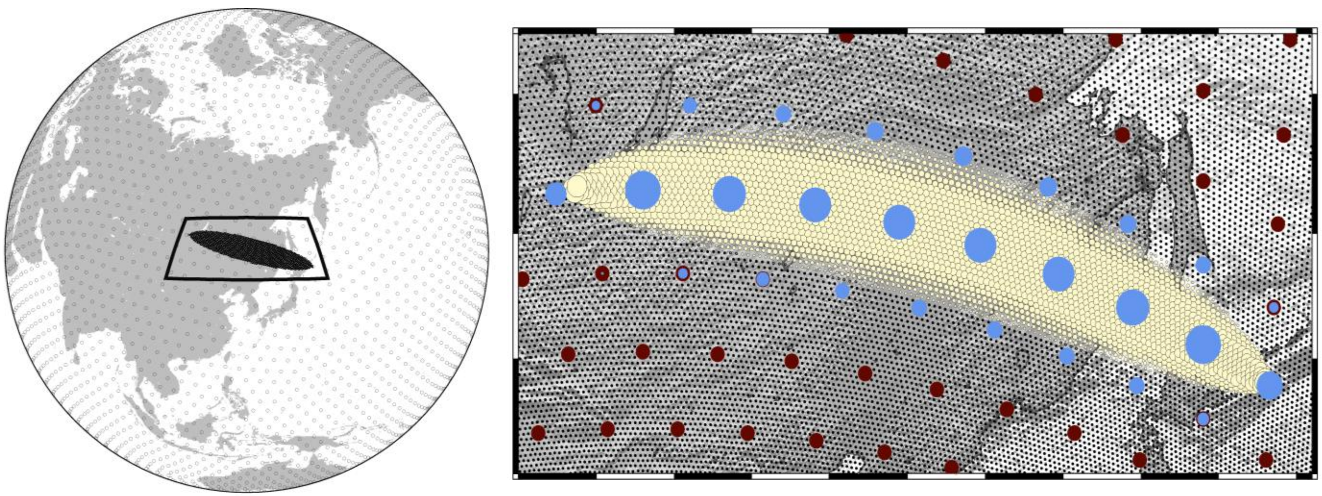

Path Weighting

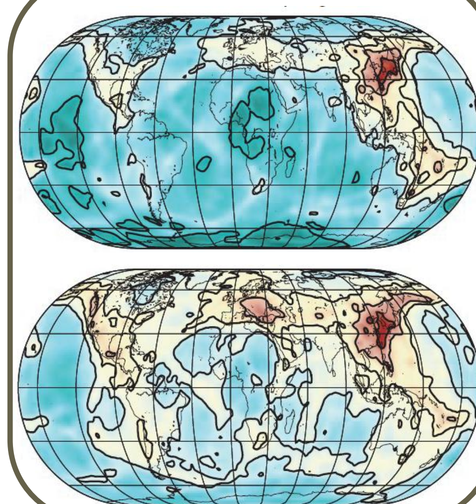

Lebedev and van der Hilst, GJI 2008

SEM resolution test

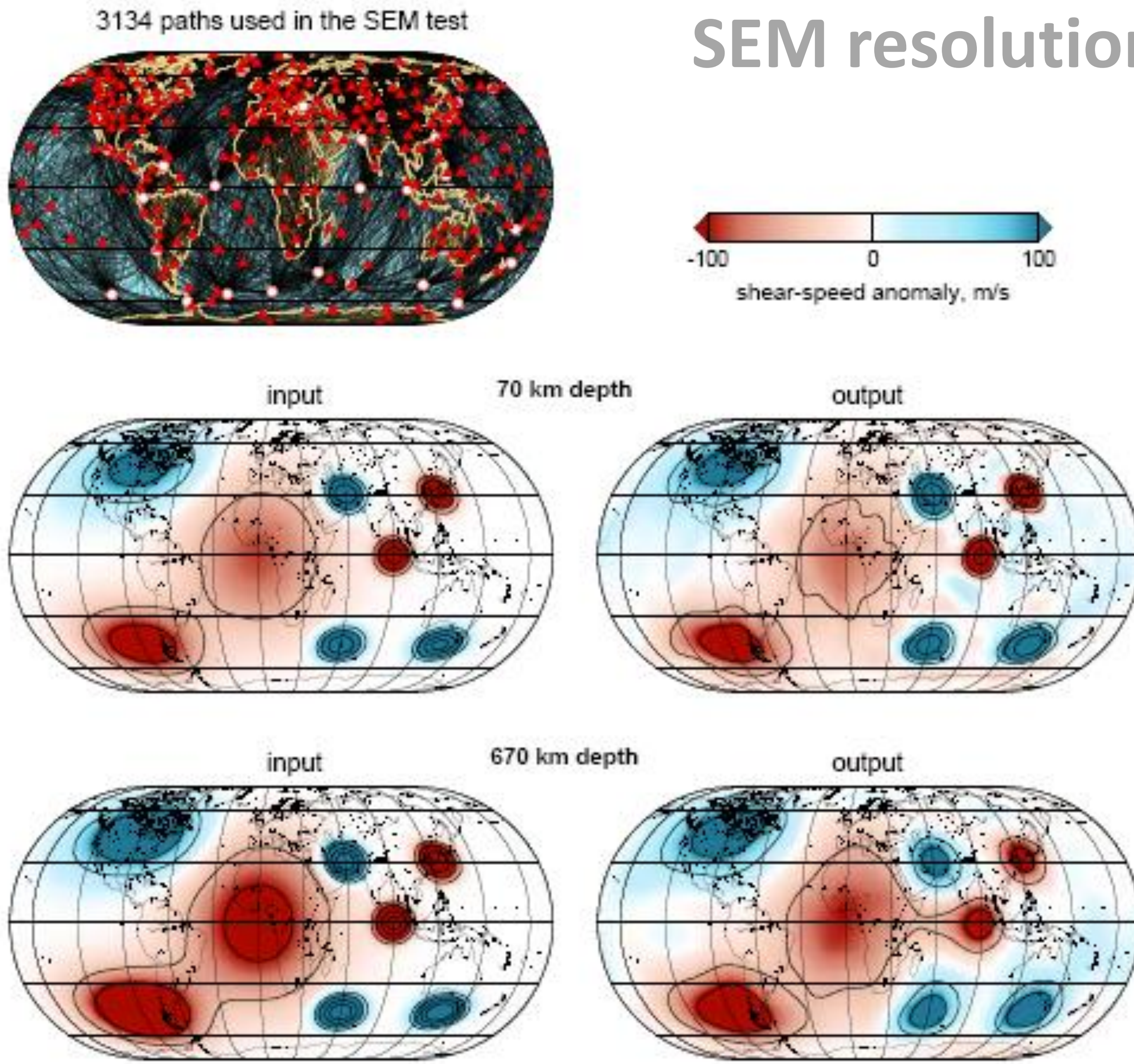

Qin et al (2006), Lebedev & van der Hilst (2008)

Earth's upper mantle

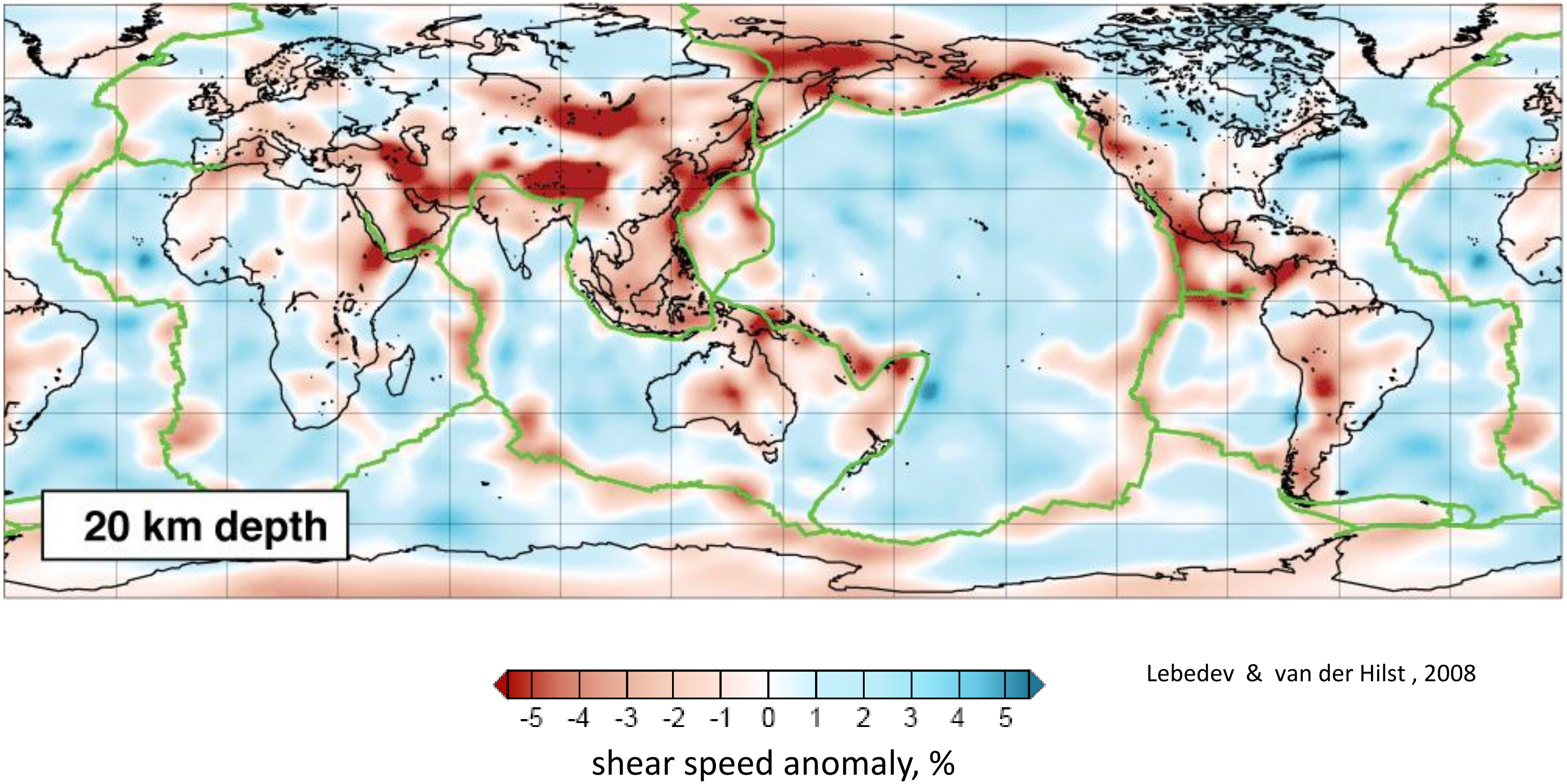

Lebedev & van der Hilst , 2008

New global model of the upper mantle

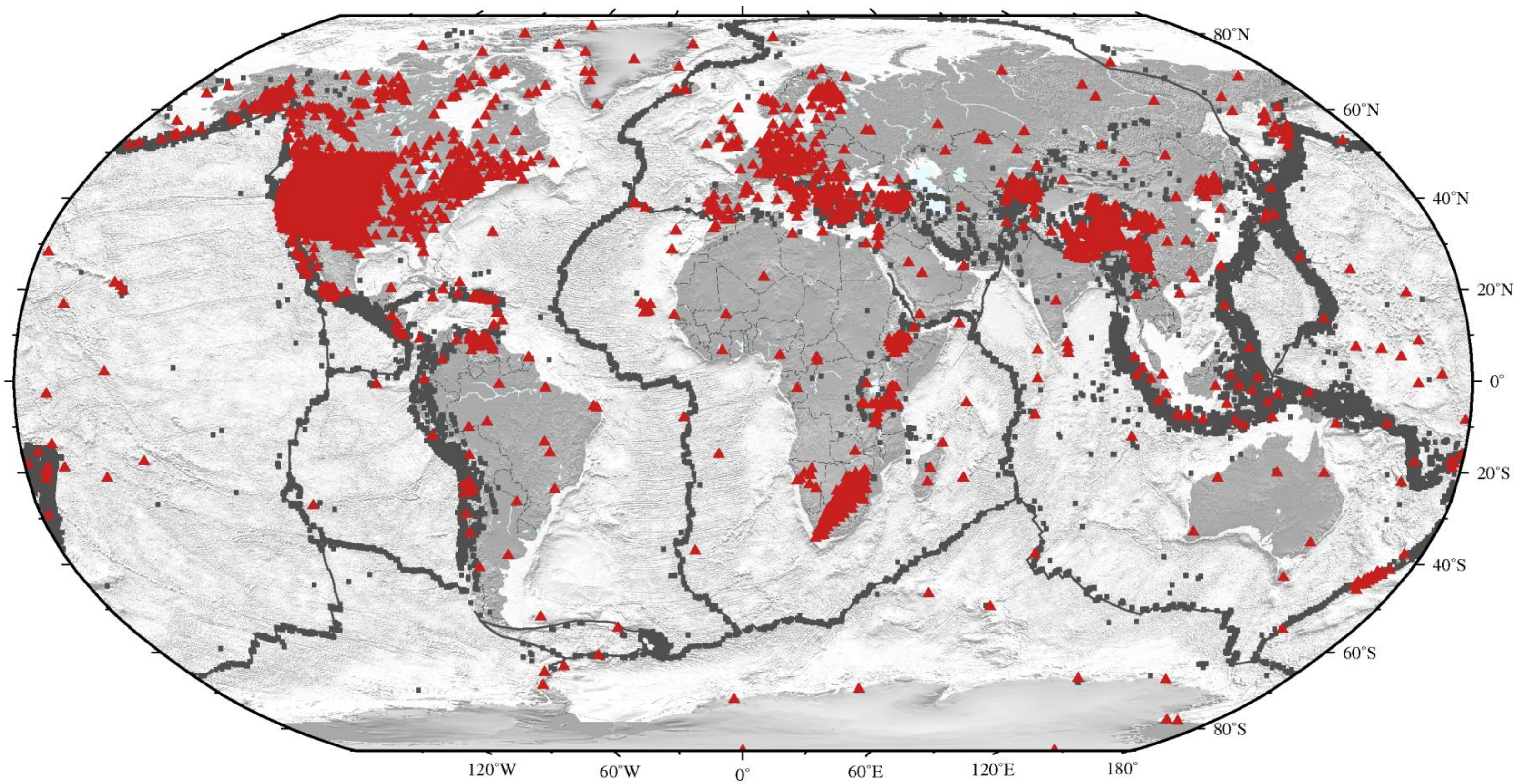

Ph.D. Research of Andrew Schaeffer (DIAS)

- **1 Million** seismograms successfully fit using AMI
  - ~750k vertical and ~250k transverse components
  - Use 550k of best fitting Rayleigh fits (based on outlier removal)
- Order of magnitude increase in number of seismograms over earlier datasets

What's in the dataset?

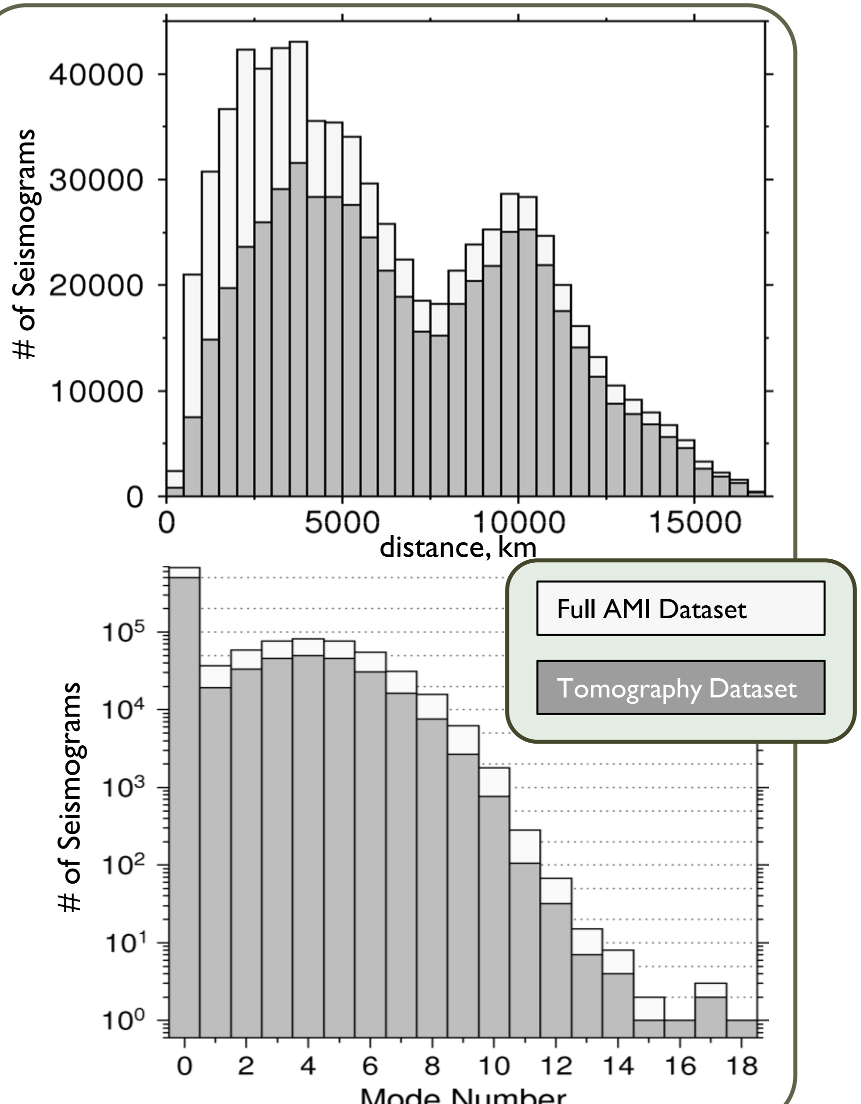

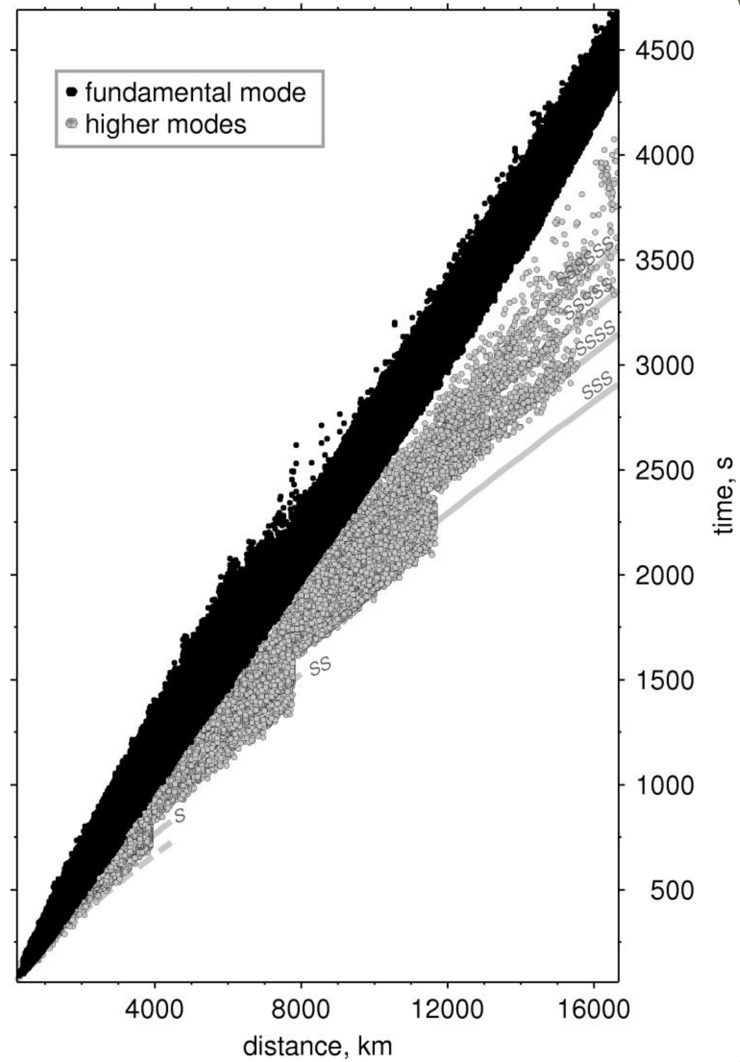

What's in the dataset?

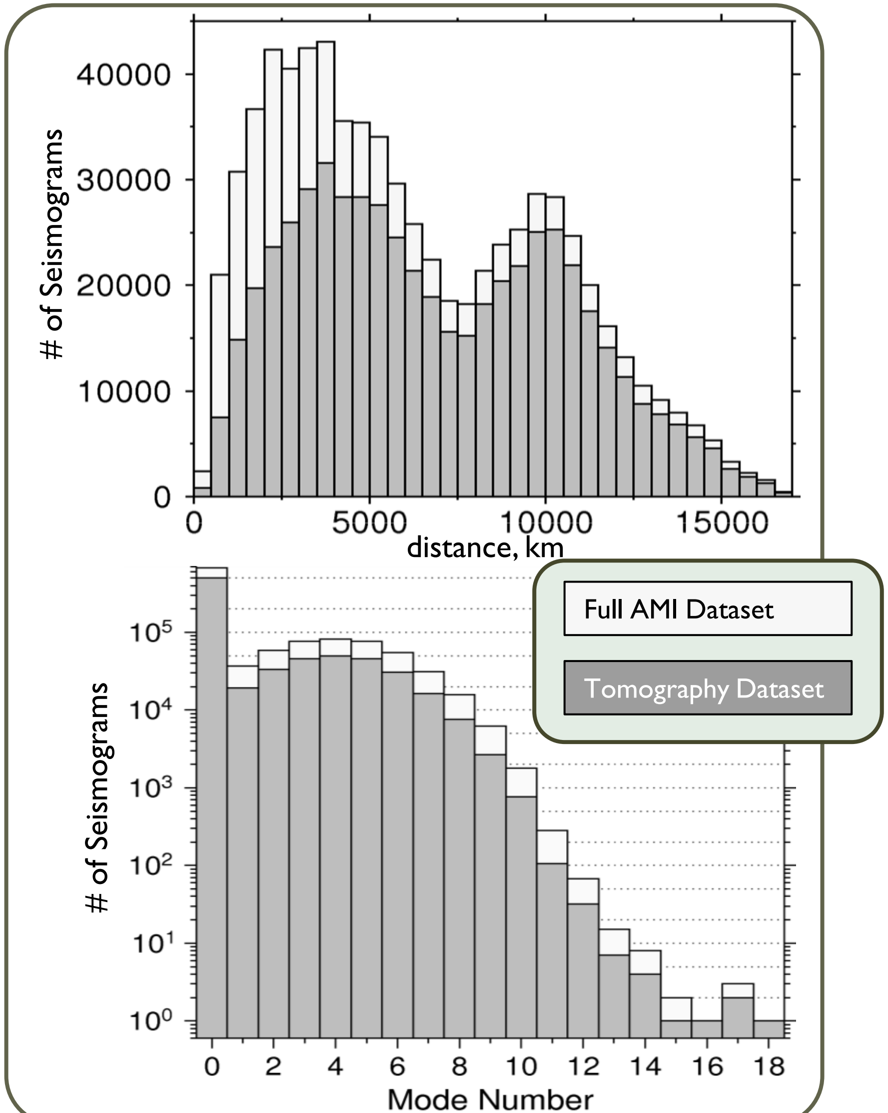

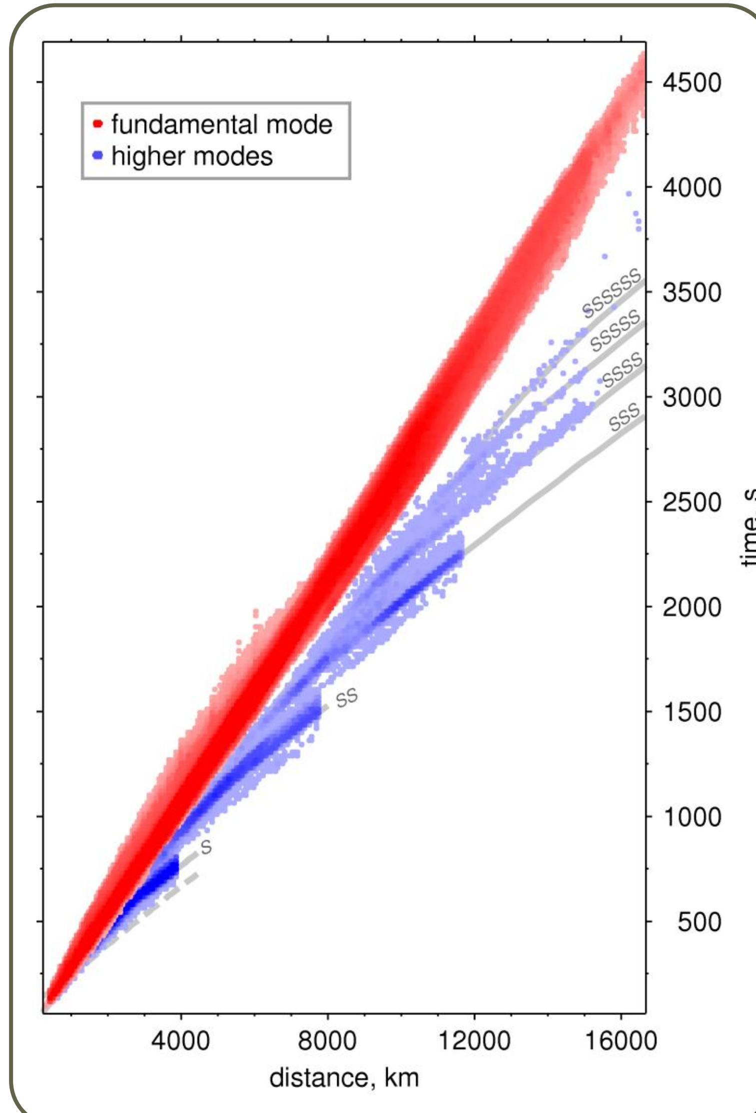

Empirical dispersion properties of the upper mantle

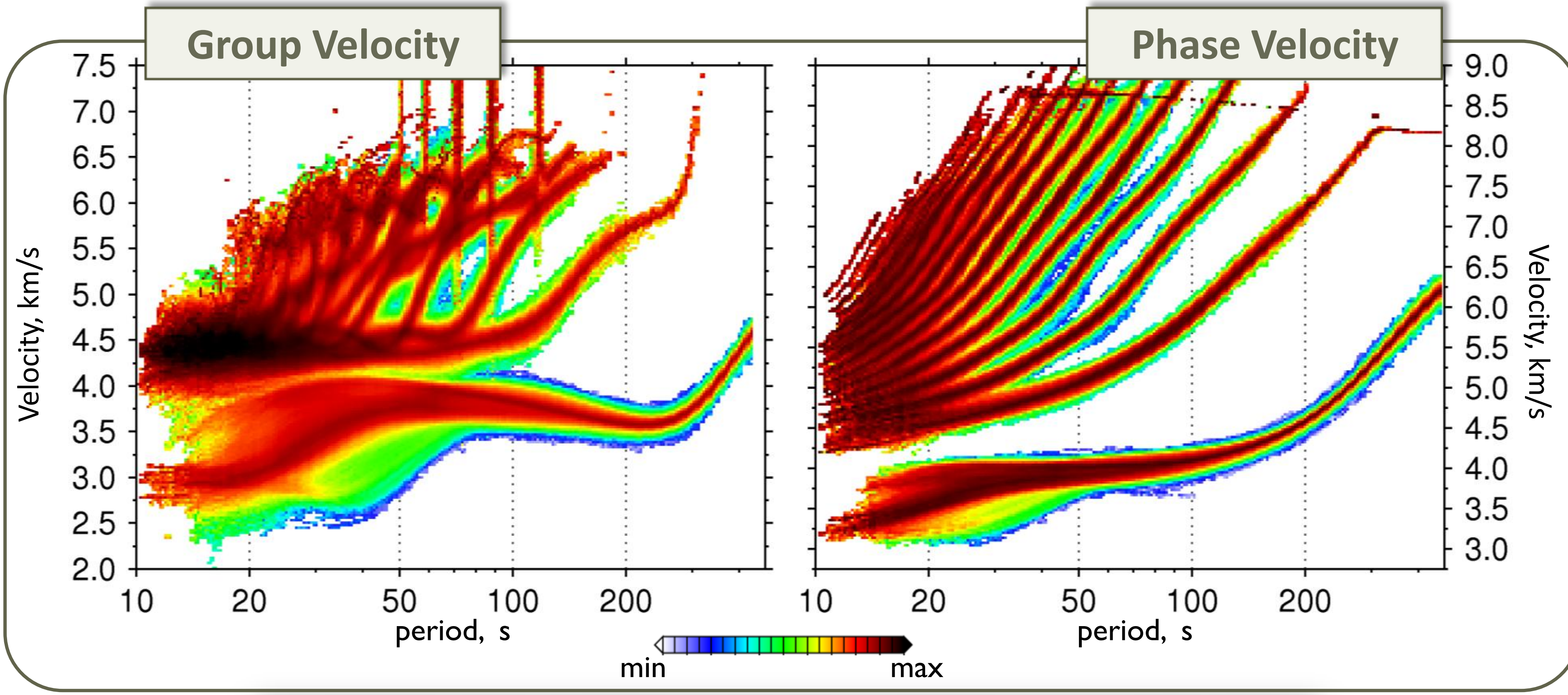

- Fundamental and Higher mode phase velocities measured by AMI
- Group Velocities computed from phase velocities
  - Modes 0 through 16
- Computed dispersion curves for for AK 135

Empirical dispersion properties of the upper mantle

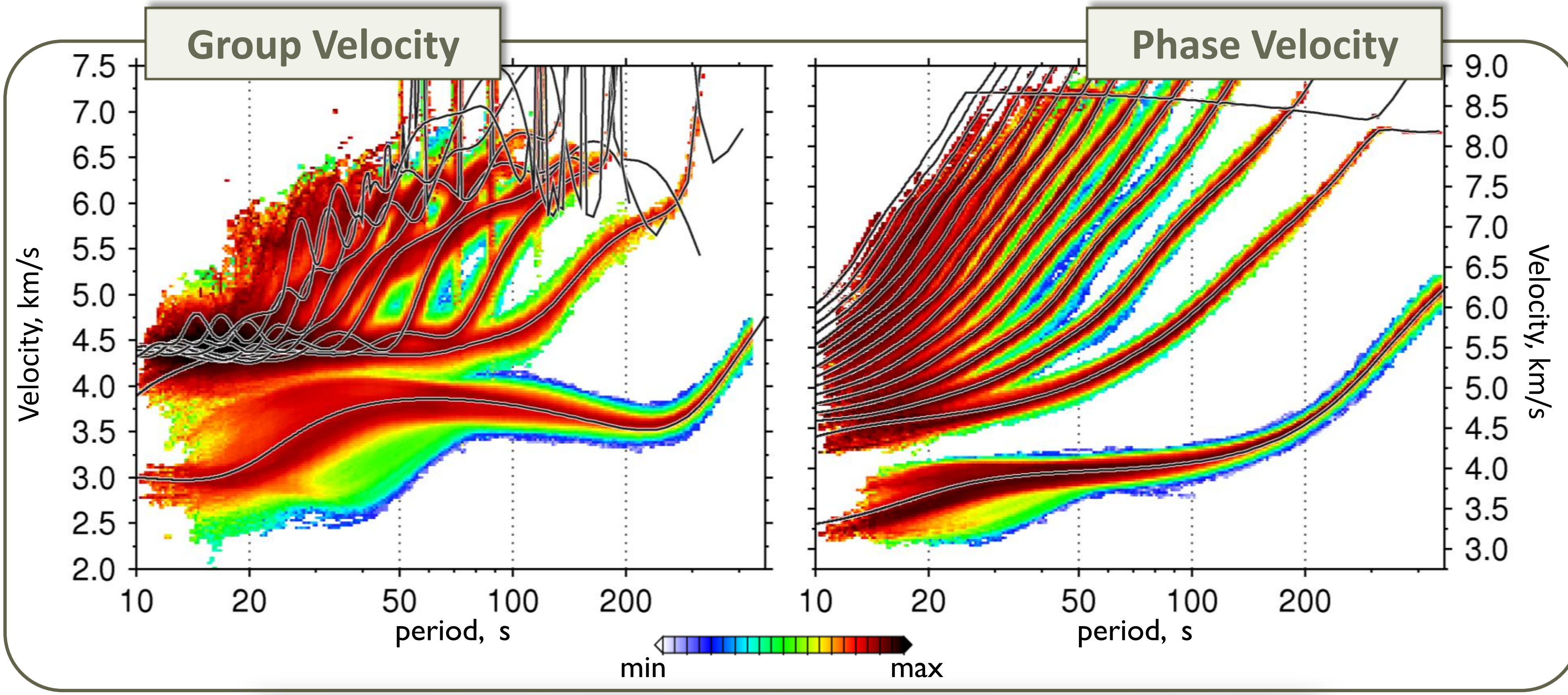

- Fundamental and Higher mode phase velocities measured by AMI
- Group Velocities computed from phase velocities
  - Modes 0 through 16
- Computed dispersion curves for for AK 135

Empirical Validity of Surface Wave Ray Theory

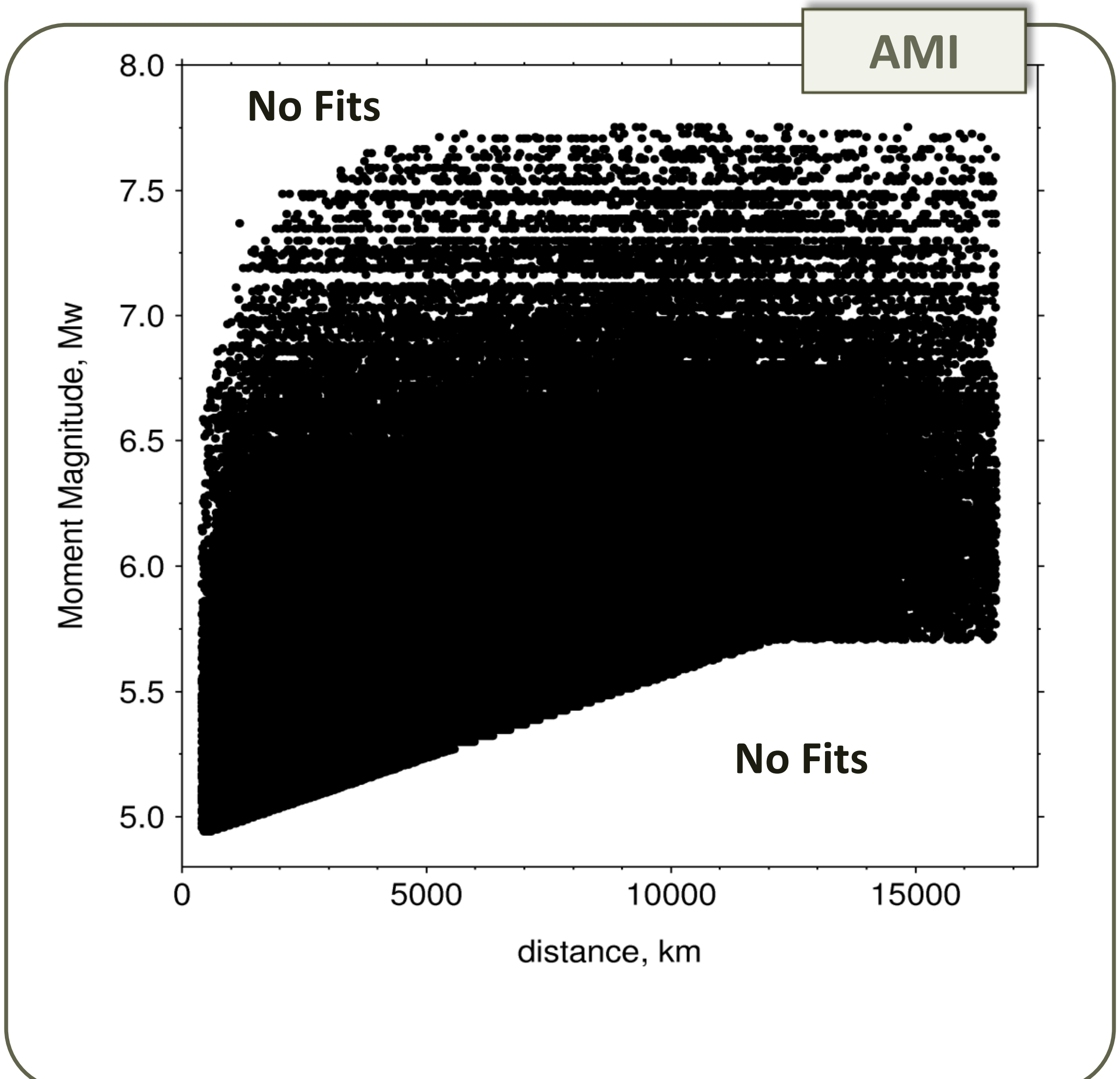

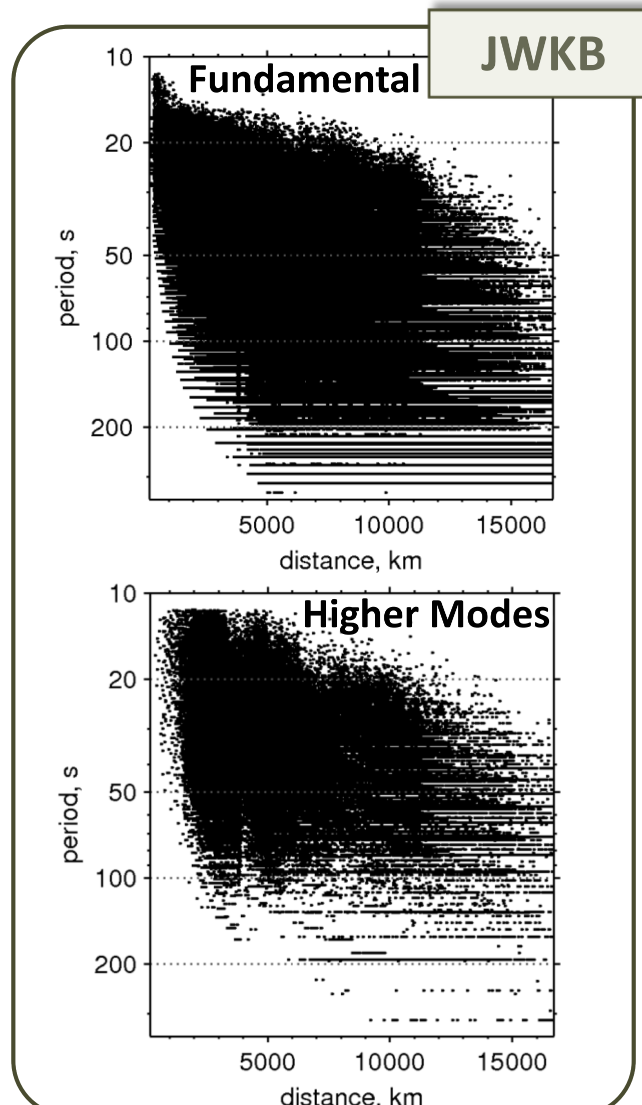

Empirical Validity of Surface Wave Ray Theory

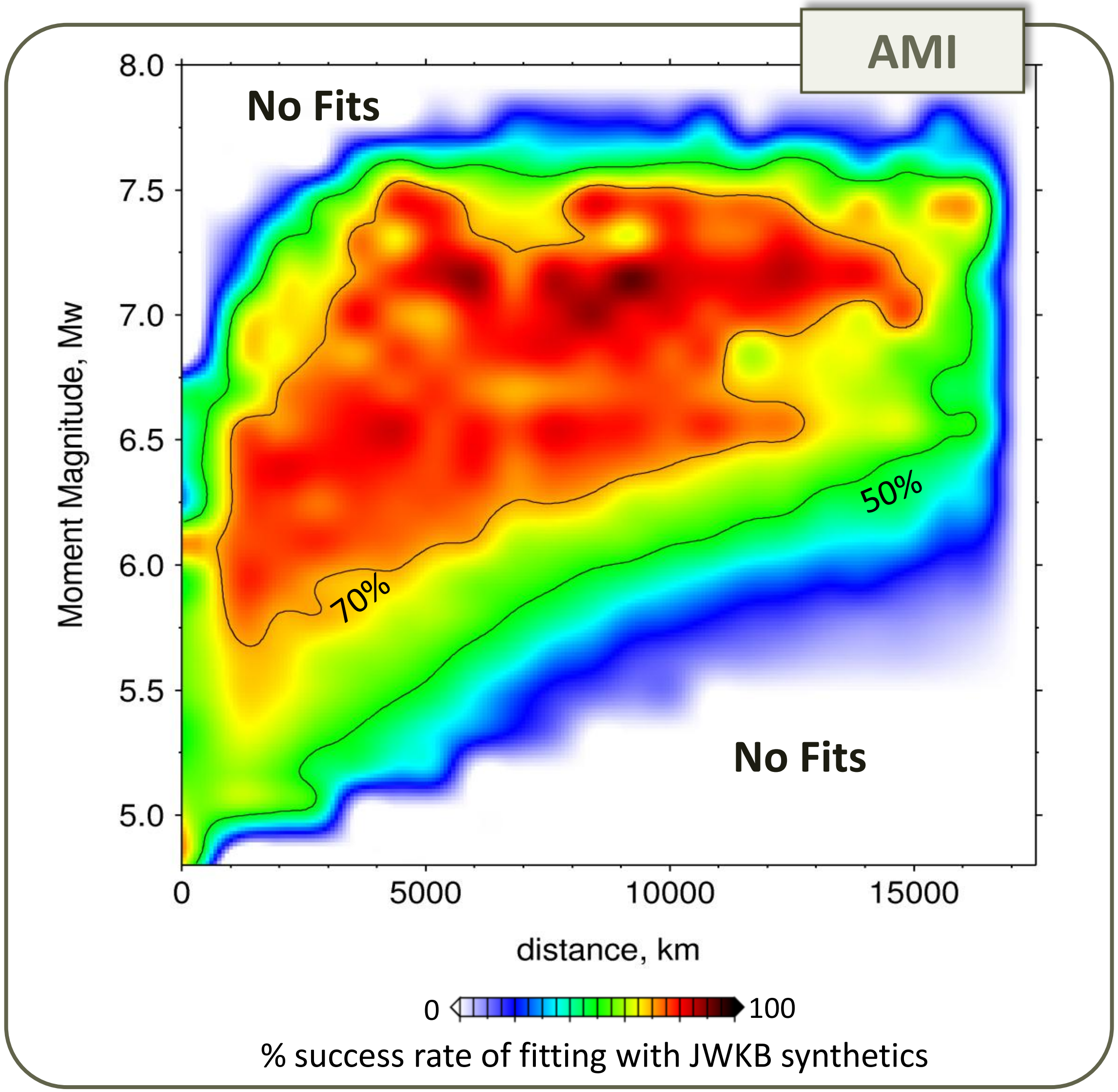

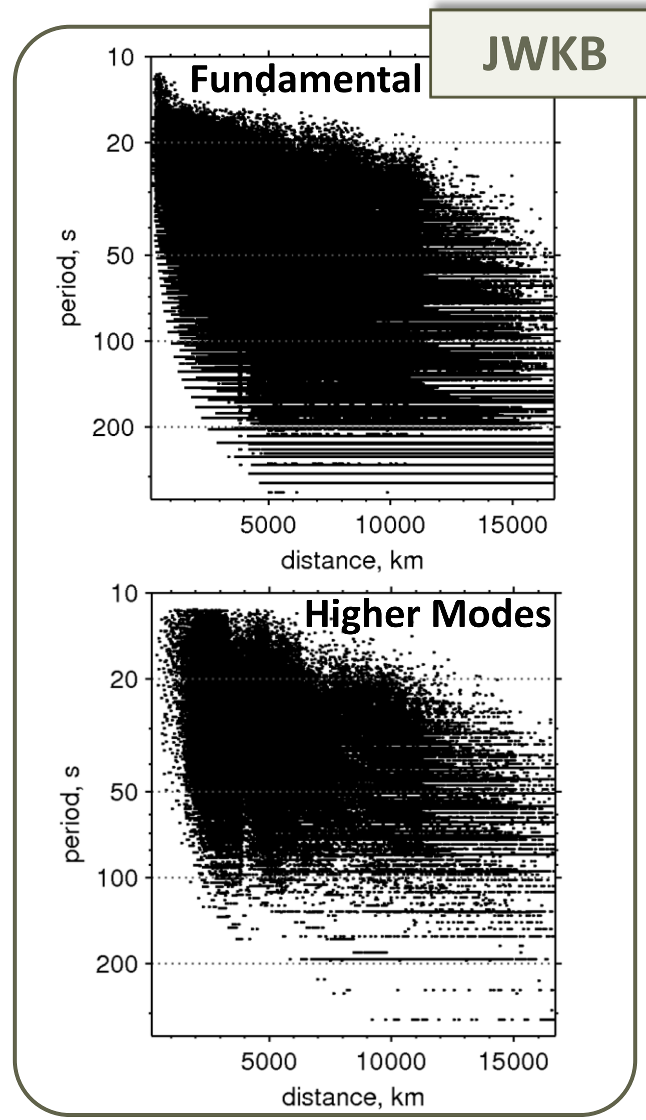

Empirical Validity of Surface Wave Ray Theory

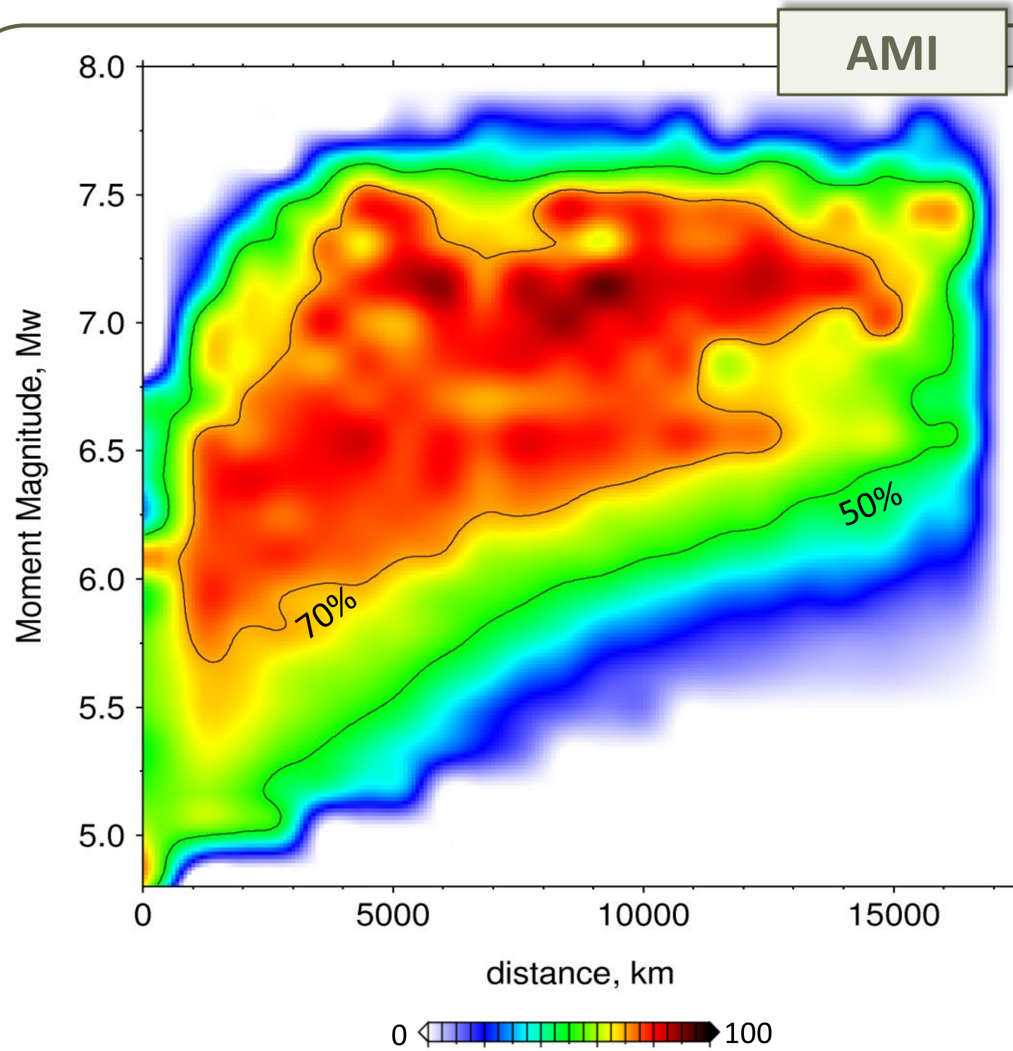

% success rate of fitting with JWKB synthetics

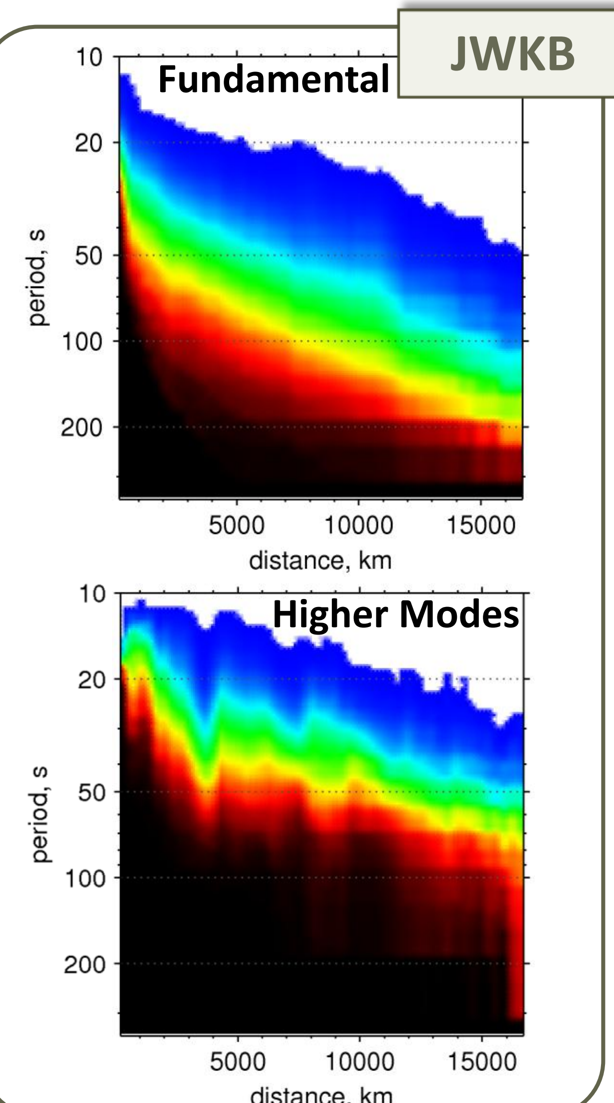

Shear-velocity structure of the upper mantle

80 km

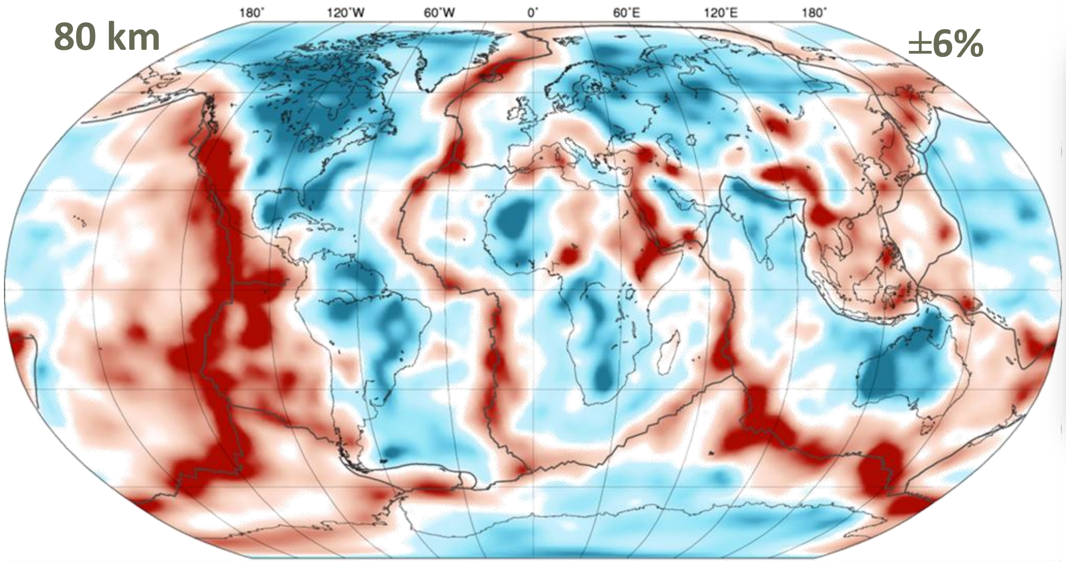

±6%

← Horizontal slice at 80 km

- Striking low velocity anomalies associated with mid-ocean ridges
- High velocity anomalies indicating shallow portions of cratonic mantle keels

Horizontal slice at 110 km →

- Dichotomy between oceans and continents
- Mid-ocean ridges still evident
- India-Asia collision
- Cameroon Line

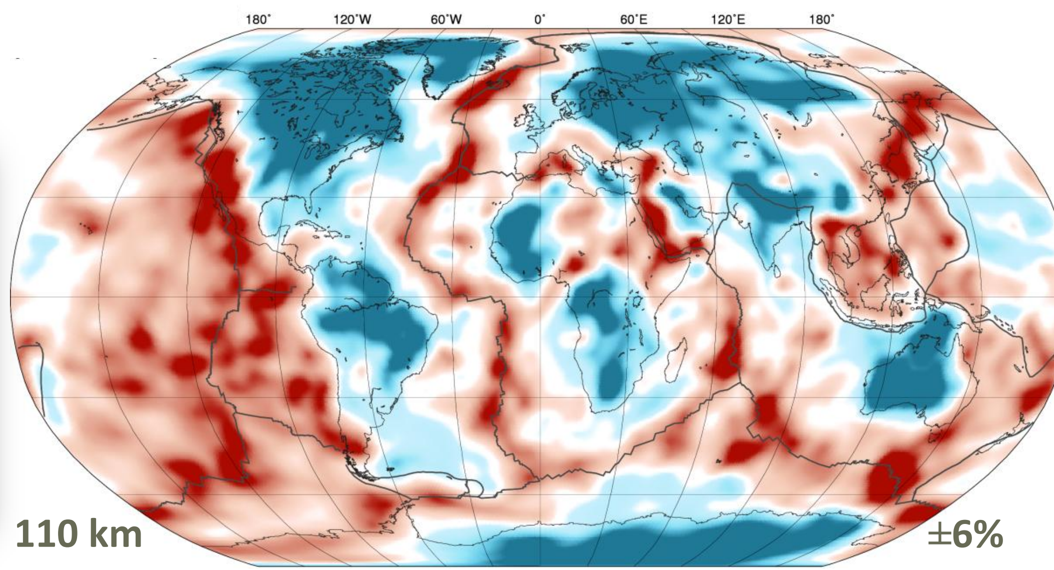

110 km

±6%

Shear-velocity structure of the upper mantle

150 km

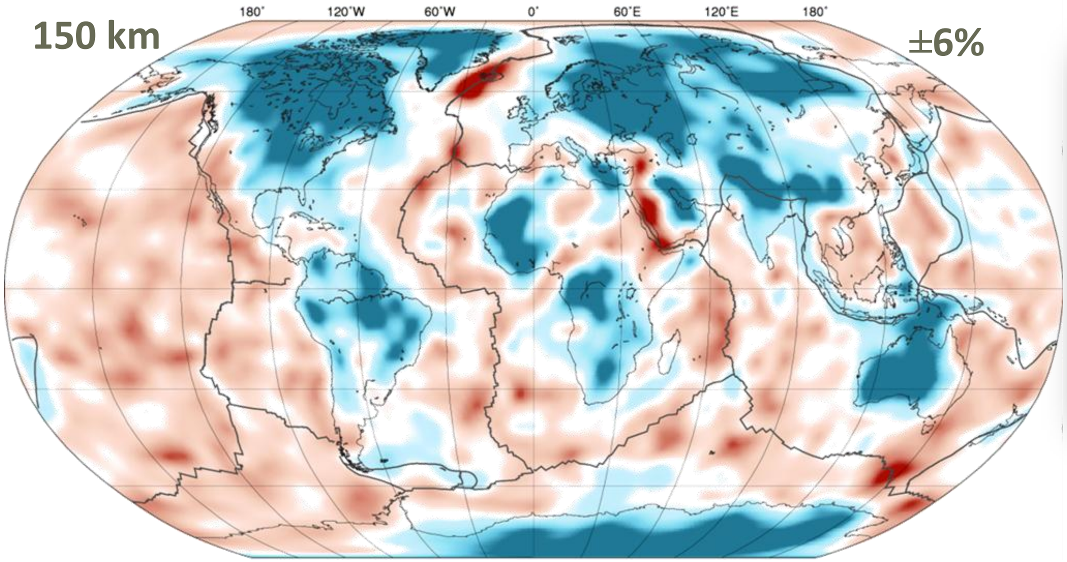

±6%

← Horizontal slice at 150 km

- Mid-ocean ridge anomalies gone (extend to ~120 km depth only)
- Dominated by fast, cold roots of continental cratons

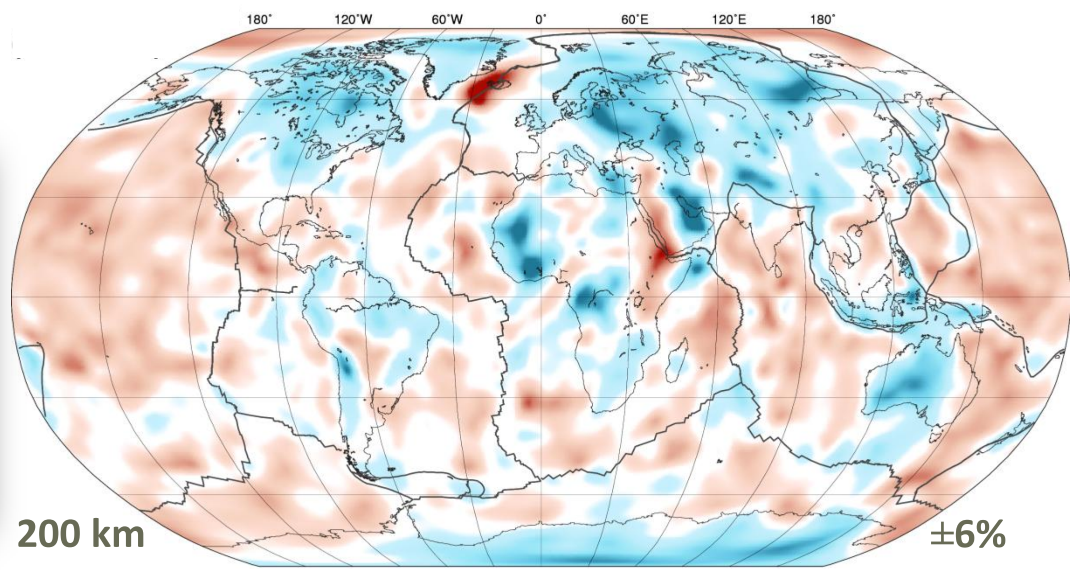

200 km

±6%

Horizontal slice at 200 km →

- Strength of heterogeneity weakened
- High velocity anomalies at the base of continental roots
- Evidence for subduction zones

Azimuthal Anisotropy

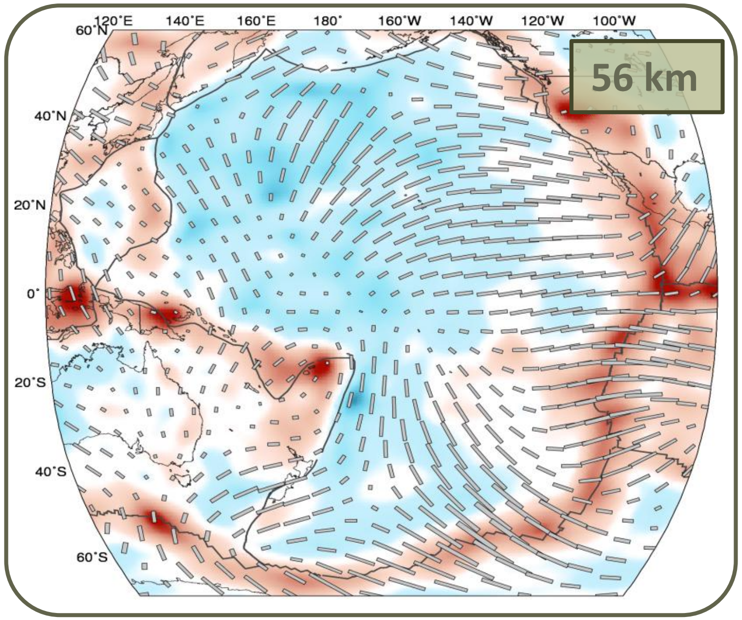

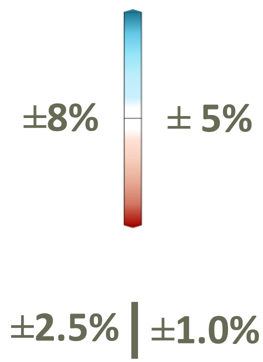

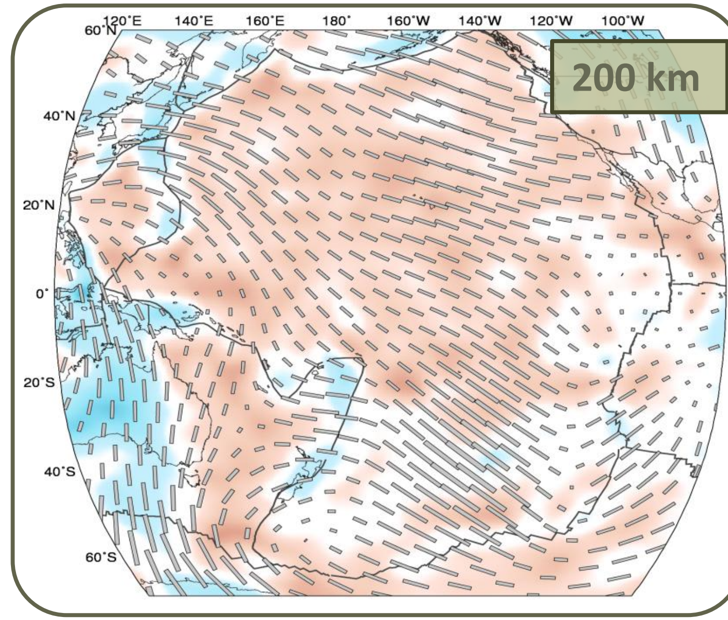

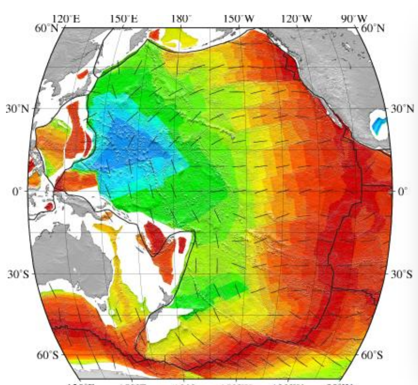

Pacific Ocean Anisotropy Stratification

- Fast axis of azimuthal anisotropy aligned with spreading direction at ridges.
- Lithosphere: frozen fabric aligns with the paleo-spreading vectors (Smith *et al.*, 2004). Anisotropy due to shearing of the uppermost mantle during spreading
- Asthenosphere: fast axis aligned with the direction of current plate motions across the entire Pacific

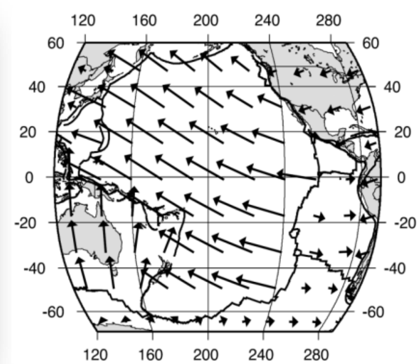

Smith *et al.*, 2004; Mueller *et al.*,. 1997

Benchmarking Magnitude of Azimuthal Anisotropy

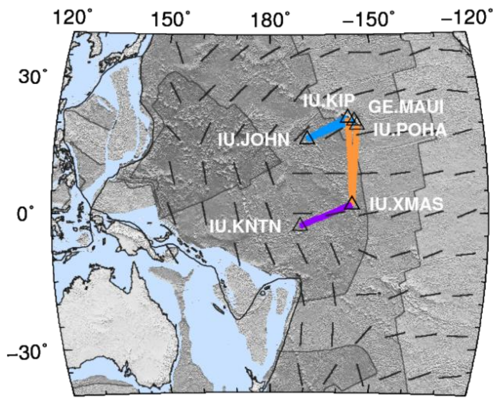

Lynch, Agius, Schaeffer, Lebedev; AGU 2011

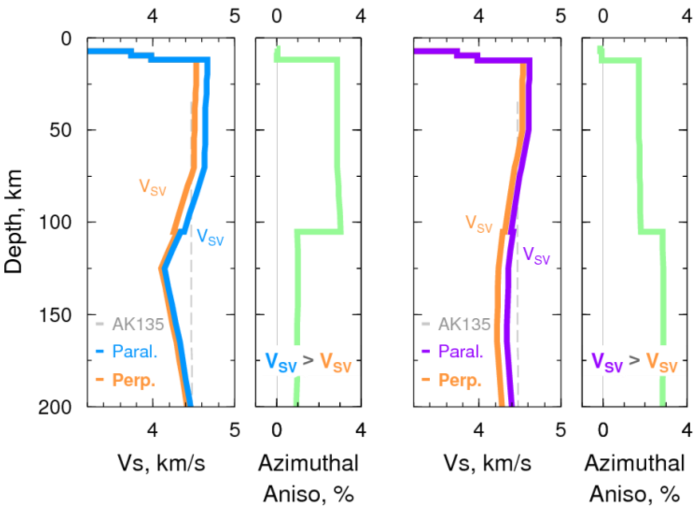

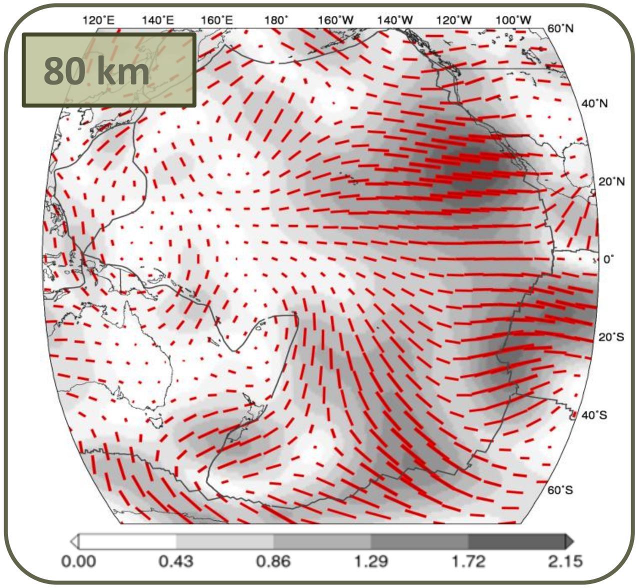

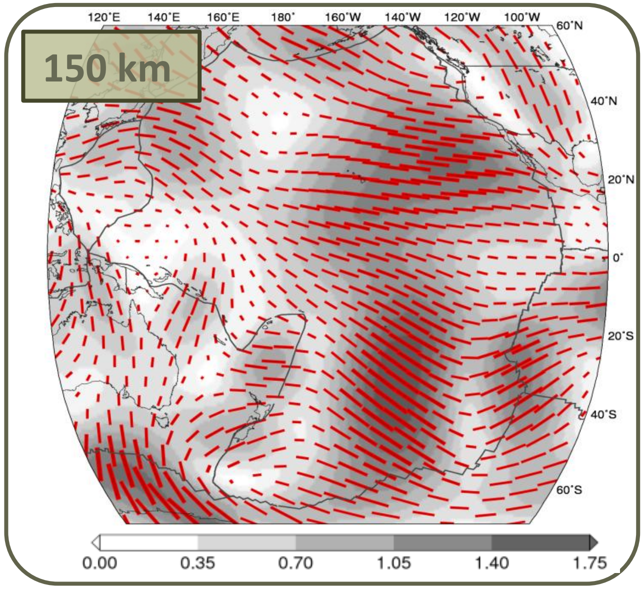

Anisotropy from Tomography vs SKS splitting

Coherence between actual SKS splitting and the splitting predicted by tomographic models

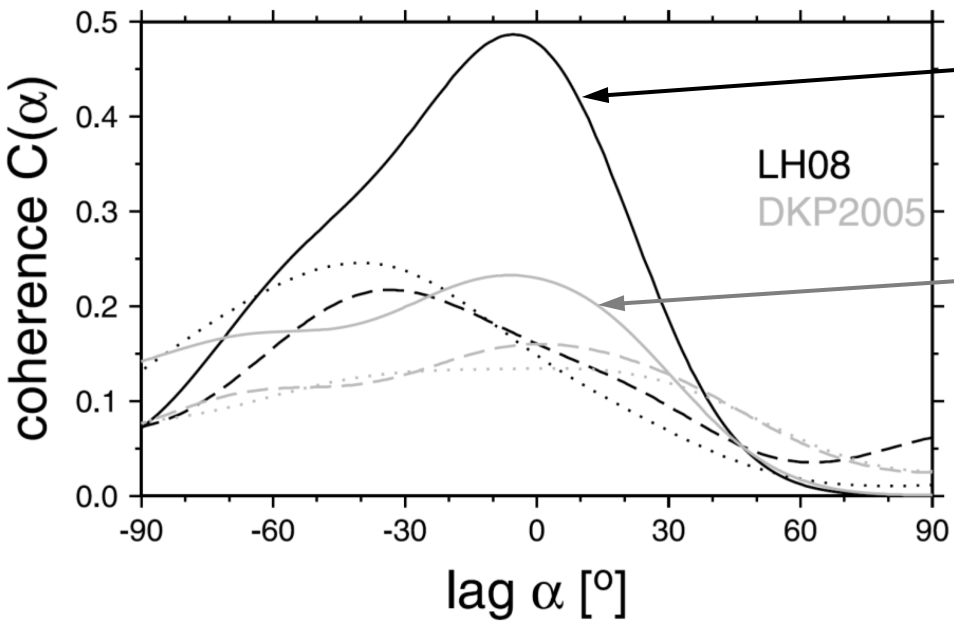

Lebedev & van der Hilst 2008

Debayle, Priestley, Kennett 2005

Spatial averaging:

solid line: bin width g = 30°;

dashed line: g = 10°;

dotted line: g = 1°

Becker, Lebedev, Long 2012

Anisotropy beneath Western North America

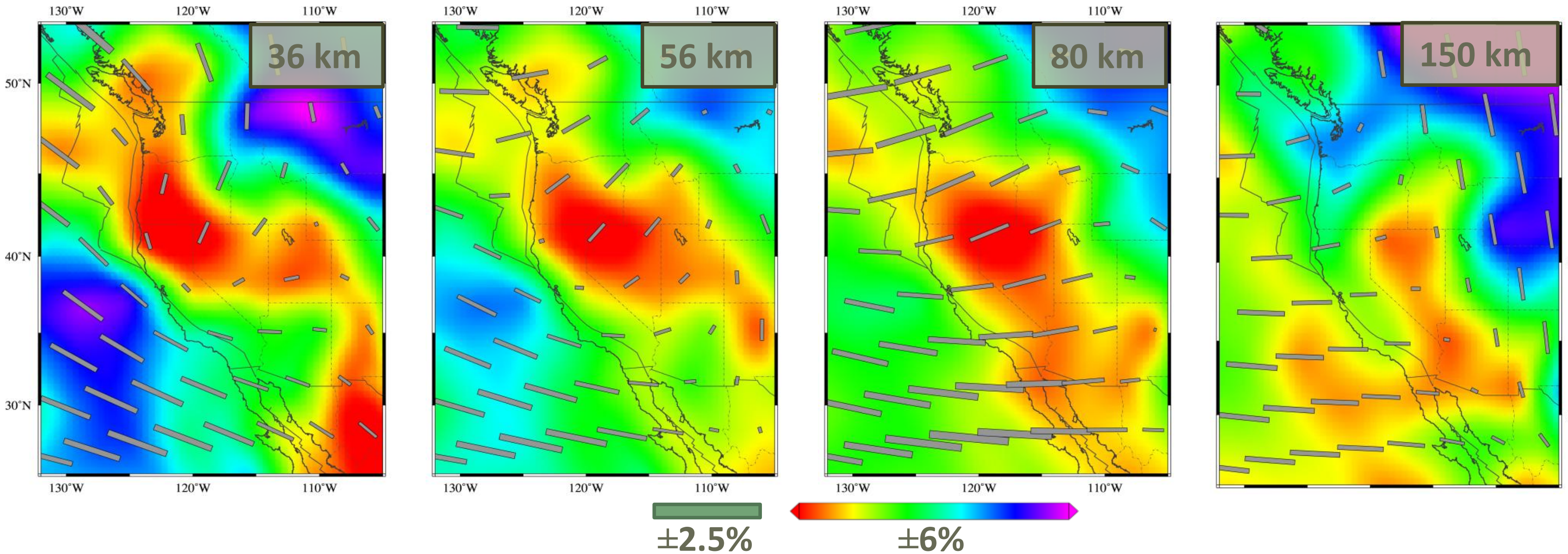

- Continental Anisotropy more complex
- Challenge for global tomography
- Complex patterns of anisotropy related to past and ongoing tectonics in western North America

Anisotropic Structure beneath Tibet and India

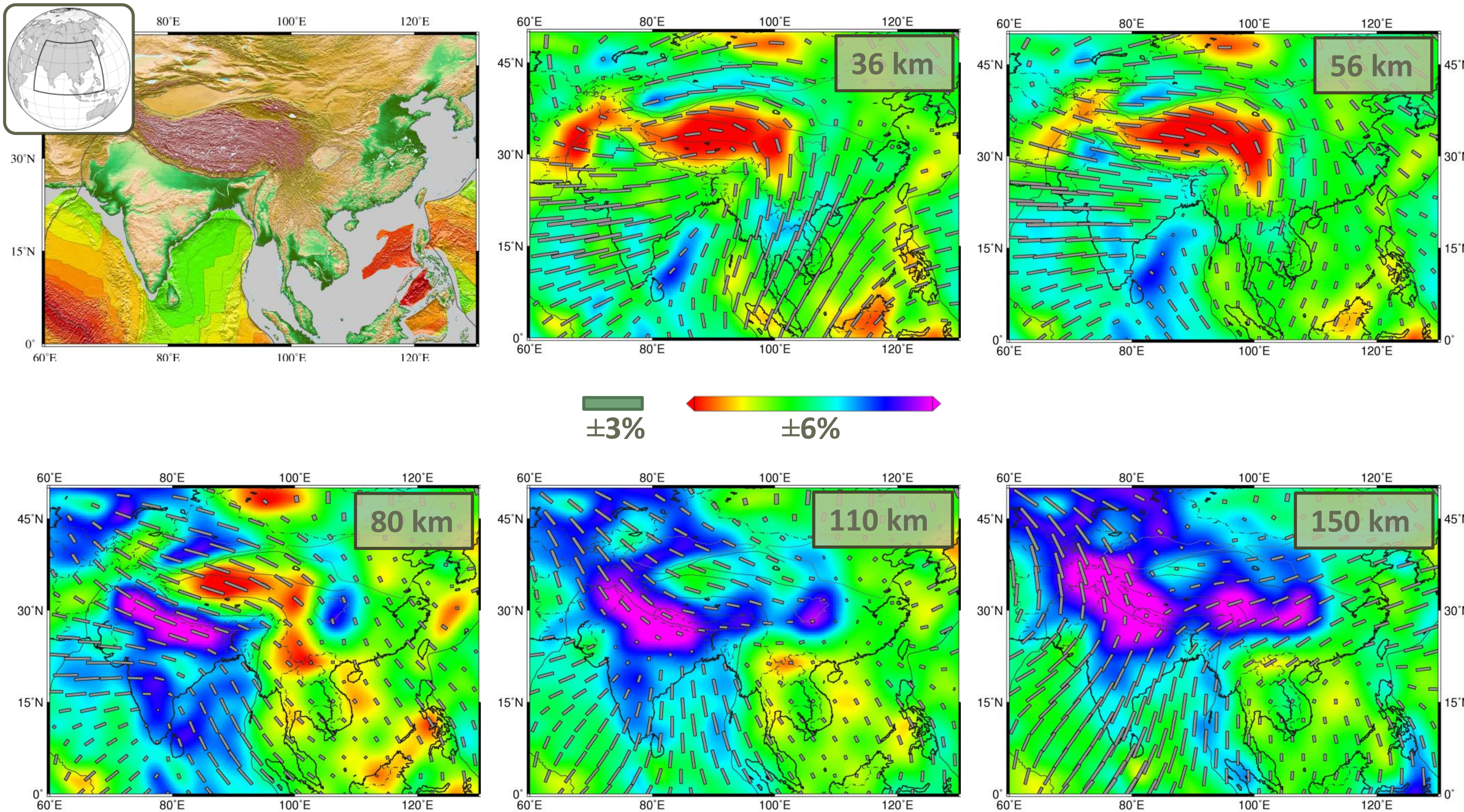

Transition Zone Structure

410 km

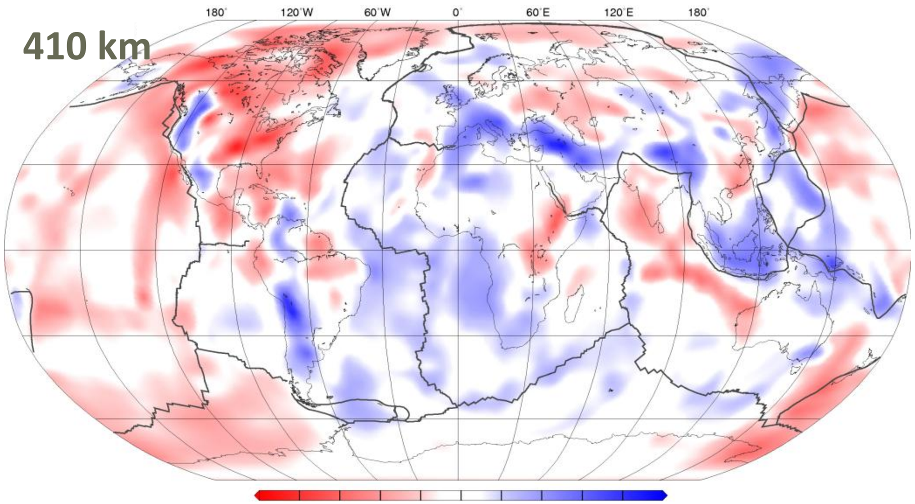

485 km

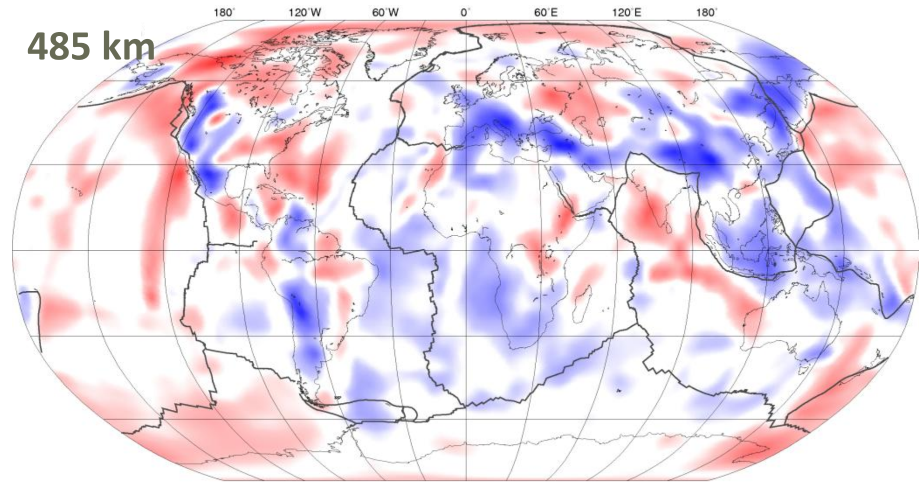

585 km

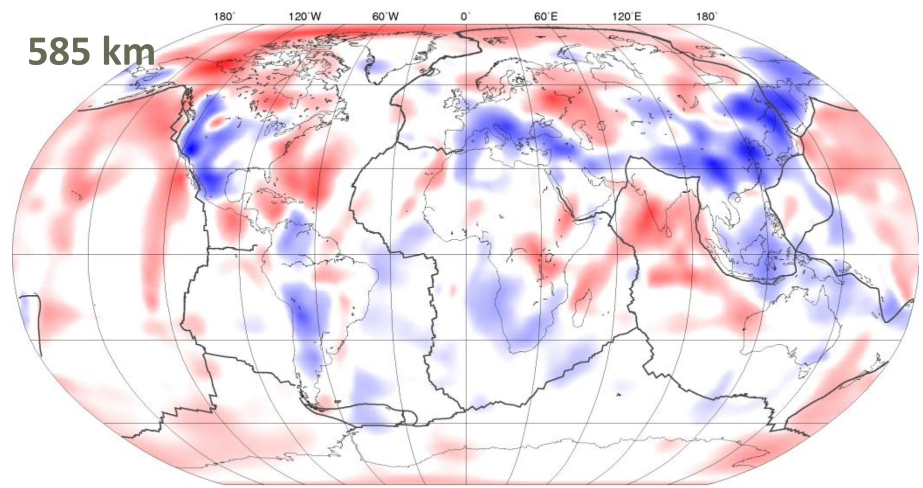

- Most major subduction zones are marked by high velocity slabs within the transition zone
- Evidence for subducted Tethyan lithosphere within the transition zone (Hafkenscheid *et al.*, 2006 (JGR))

Conclusions: Global tomography

- Spectacular growth in the amount of broadband data: opportunity for a new generation of tomographic models
- Our new dataset: multimode-waveform fits for 1 million broadband seismograms
- Our new *V*sv model: constrained by waveforms of 550 000 vertical component seismograms
- Higher resolution of upper mantle structure and anisotropy globally, compared to models of only a few years ago

II. Surface-wave array tomography

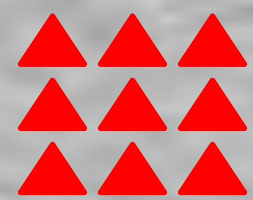

Inter-station phase-velocity measurements:

The classical two station method

- Two-station method in the frequency domain: *Sato (1955)*
- Yields an average phase-velocity curve along a path between two stations
- Needs sources on the same great circle path with the two stations
- Effects of the source mechanism and the structure away from the station pair are removed
- Surface waves should not be strongly diffracted; the method is not applicable at periods below 15-20 s

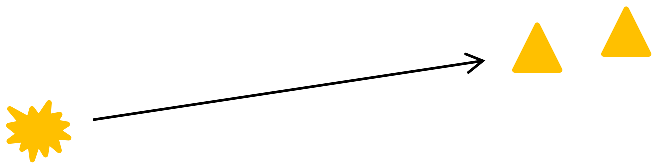

Inter-station phase-velocity measurements

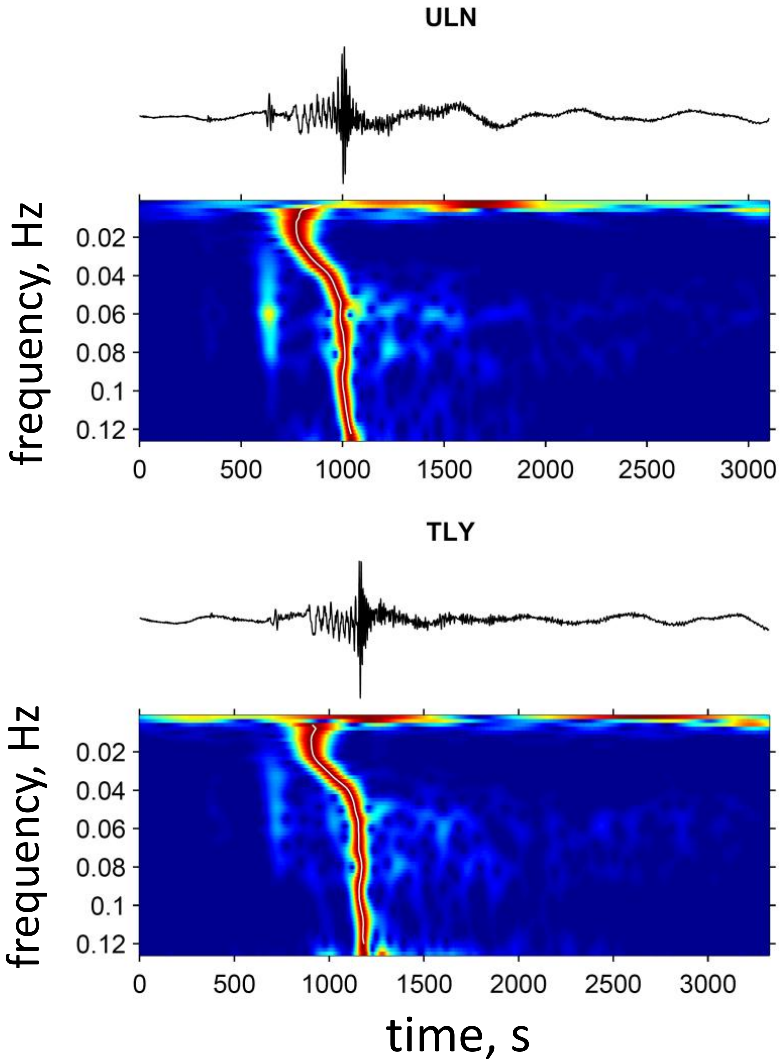

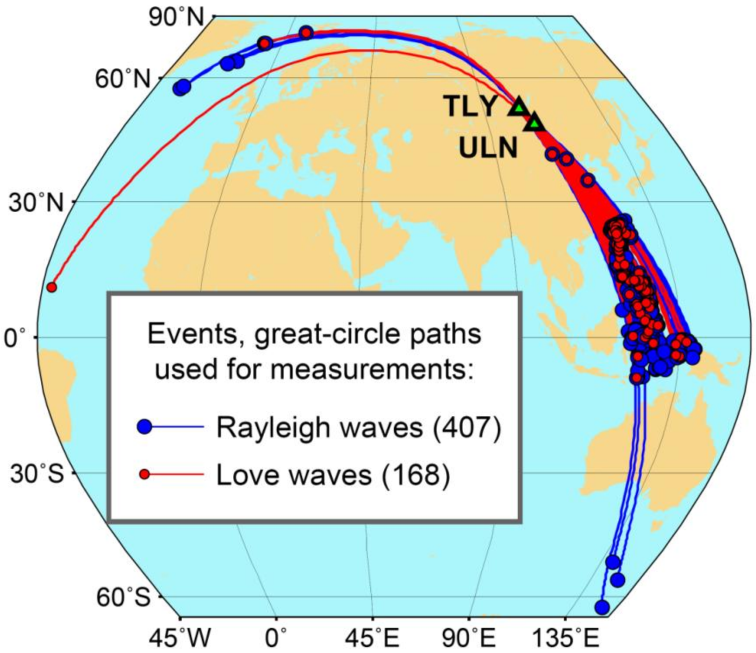

Inter-station phase-velocity measurements

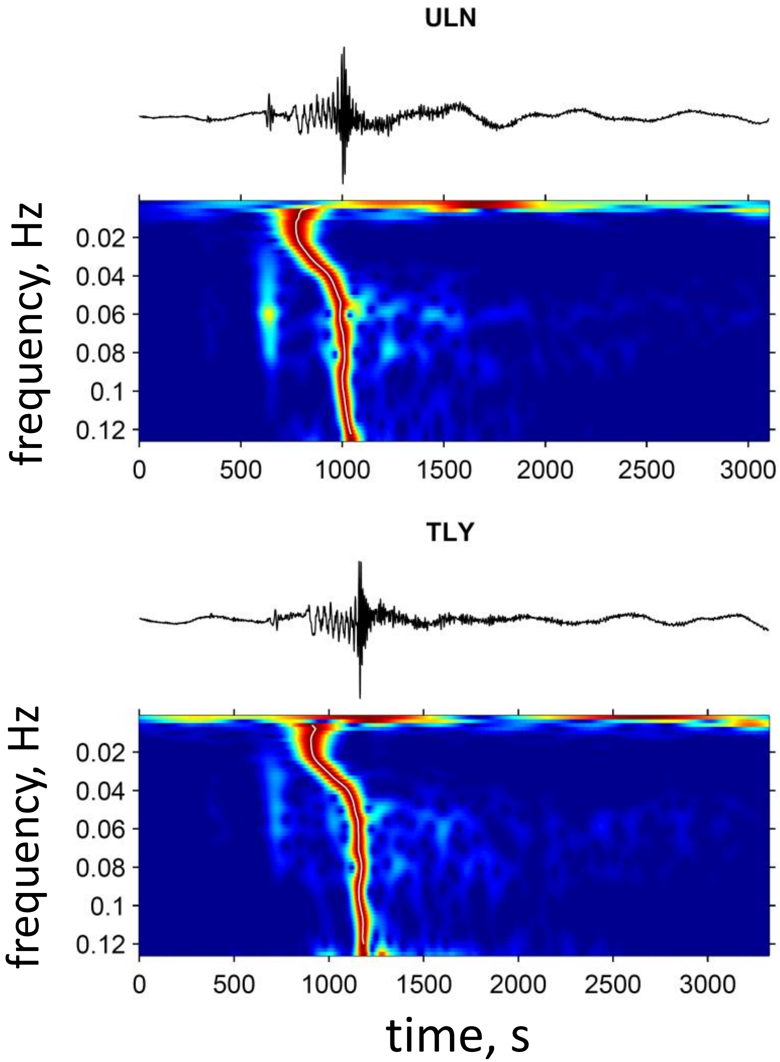

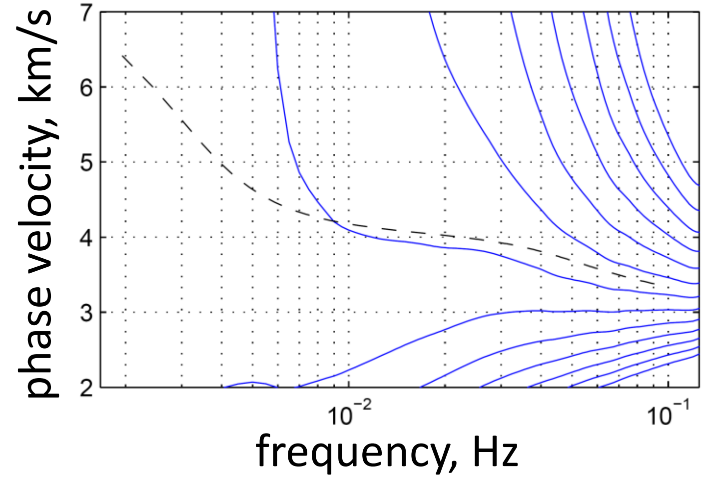

$$c(\omega) = \frac{\omega(\Delta_1 - \Delta_2)}{\arctan\{\Im[\Phi(\omega)]/\Re[\Phi(\omega)]\} + 2n\pi}$$

Meier et al., 2004

Inter-station phase-velocity measurements

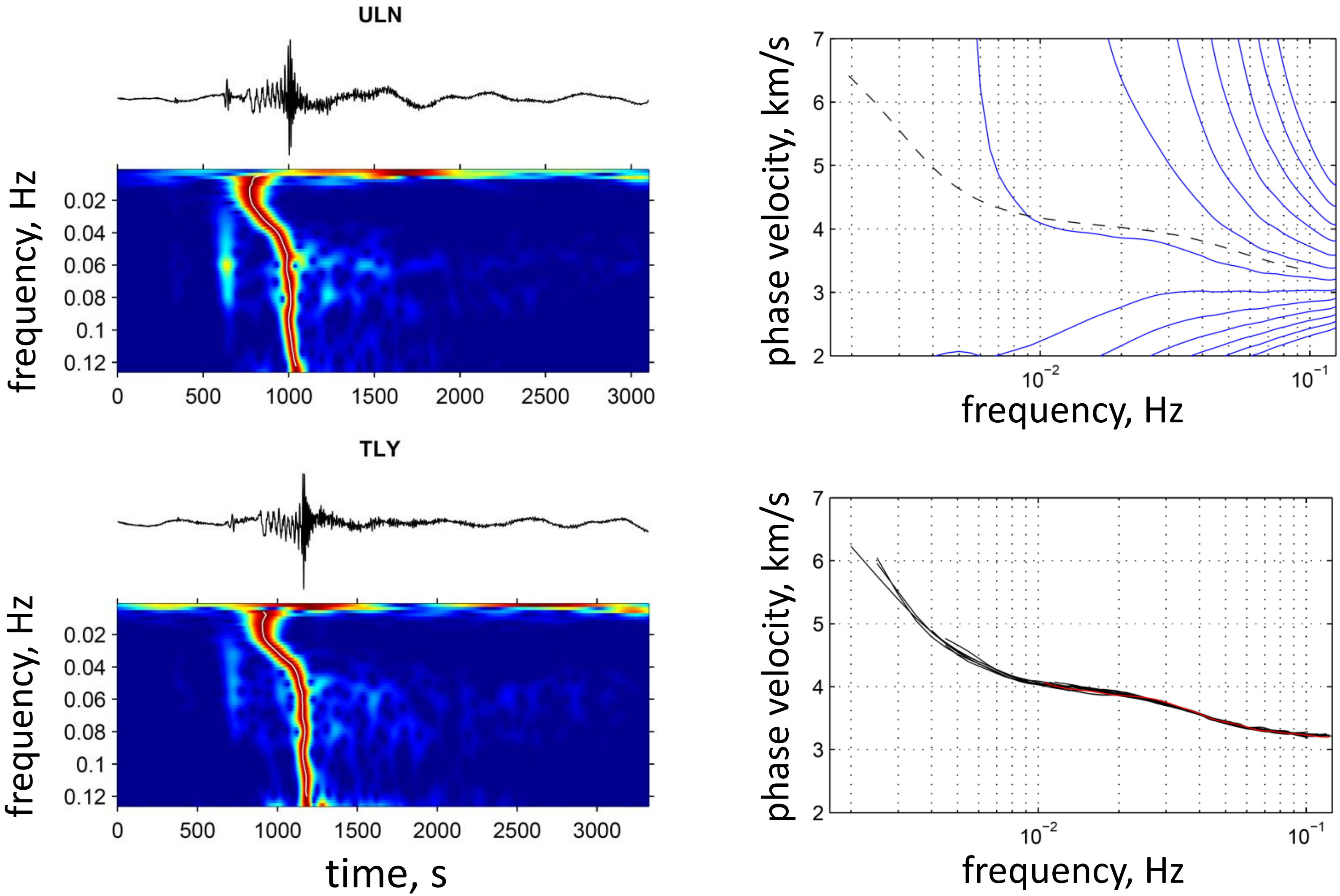

Meier et al., 2004

Cross-correlating diffracted waves

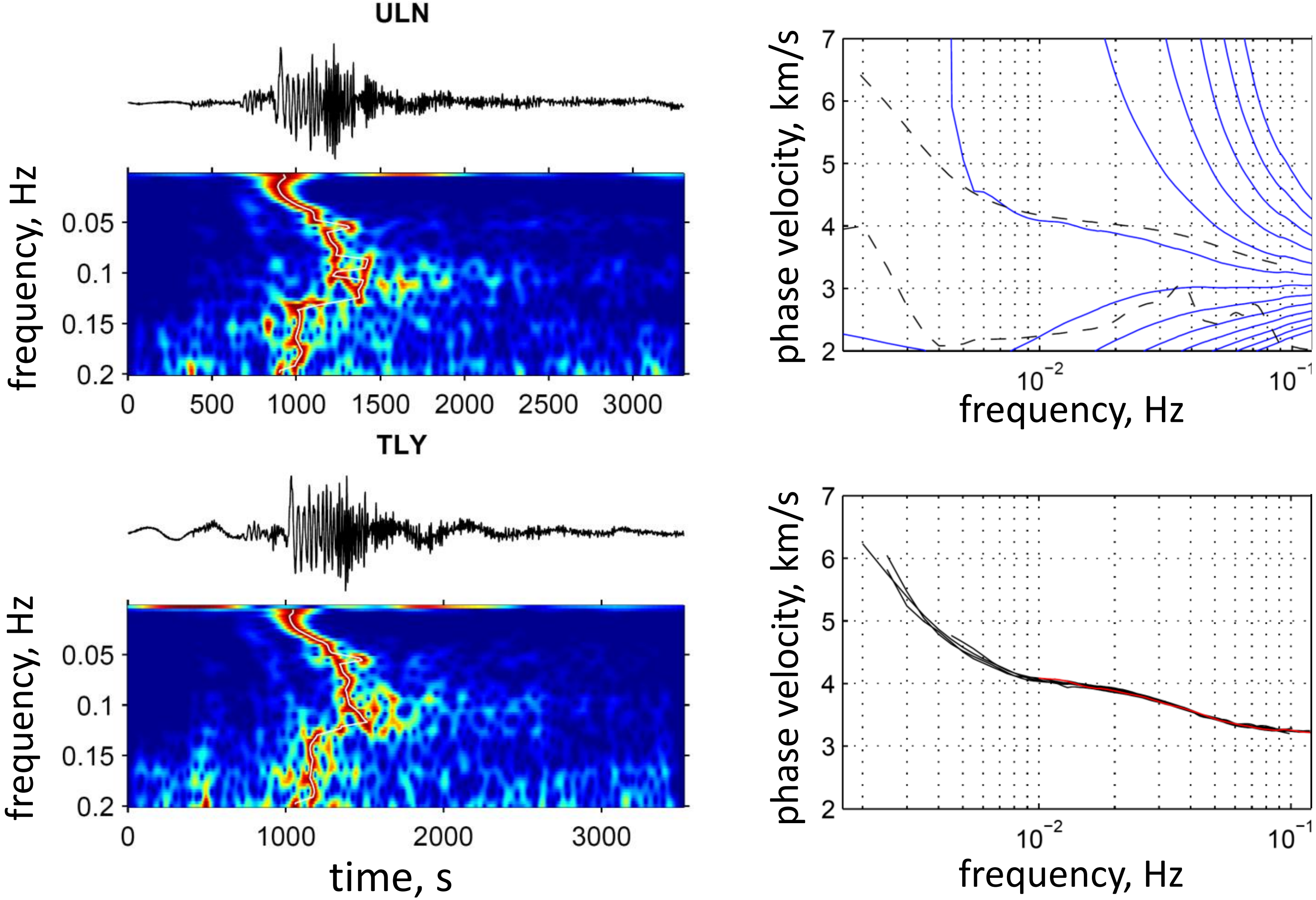

Meier et al., 2004

Cross-correlating diffracted waves

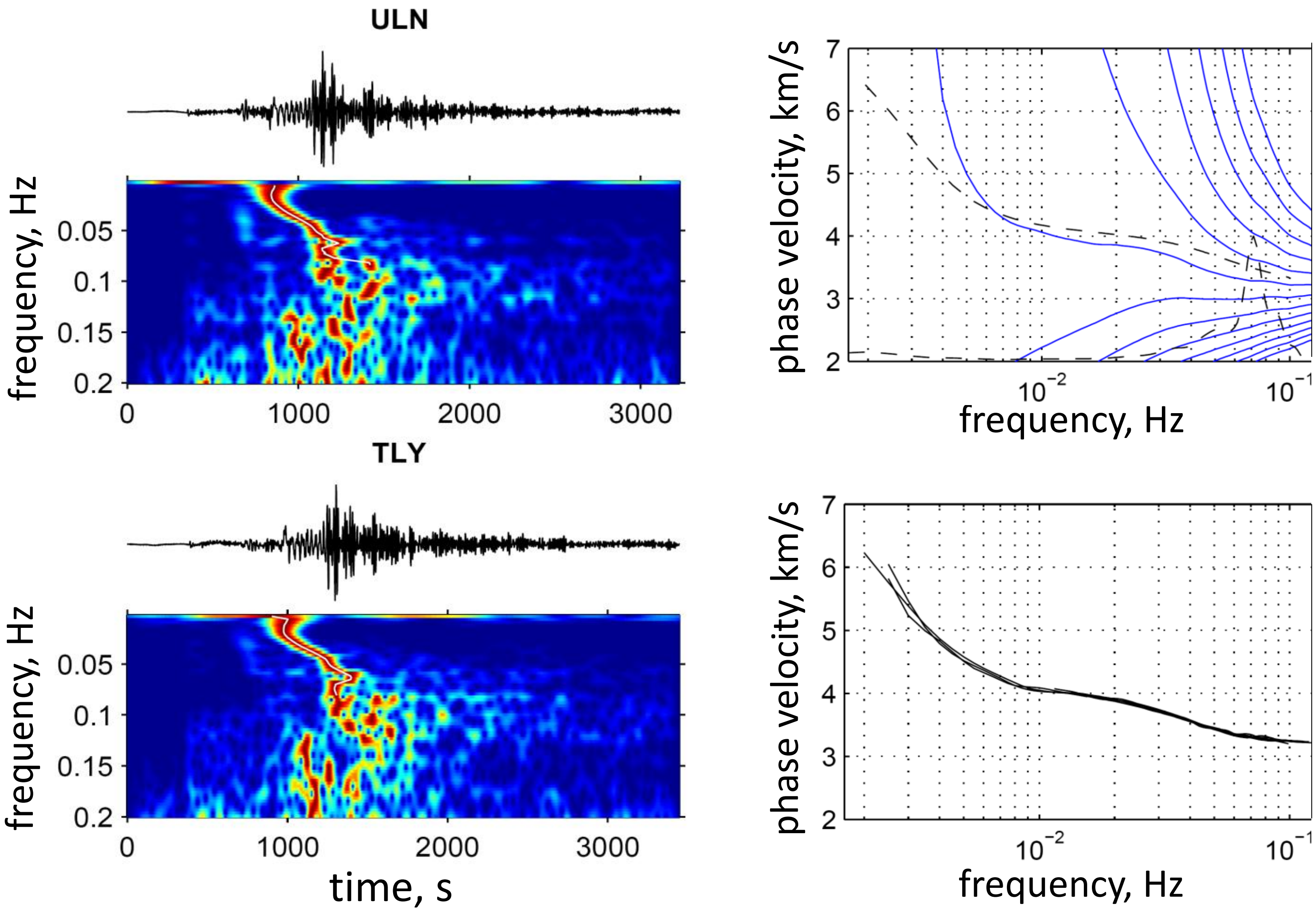

Meier et al., 2004

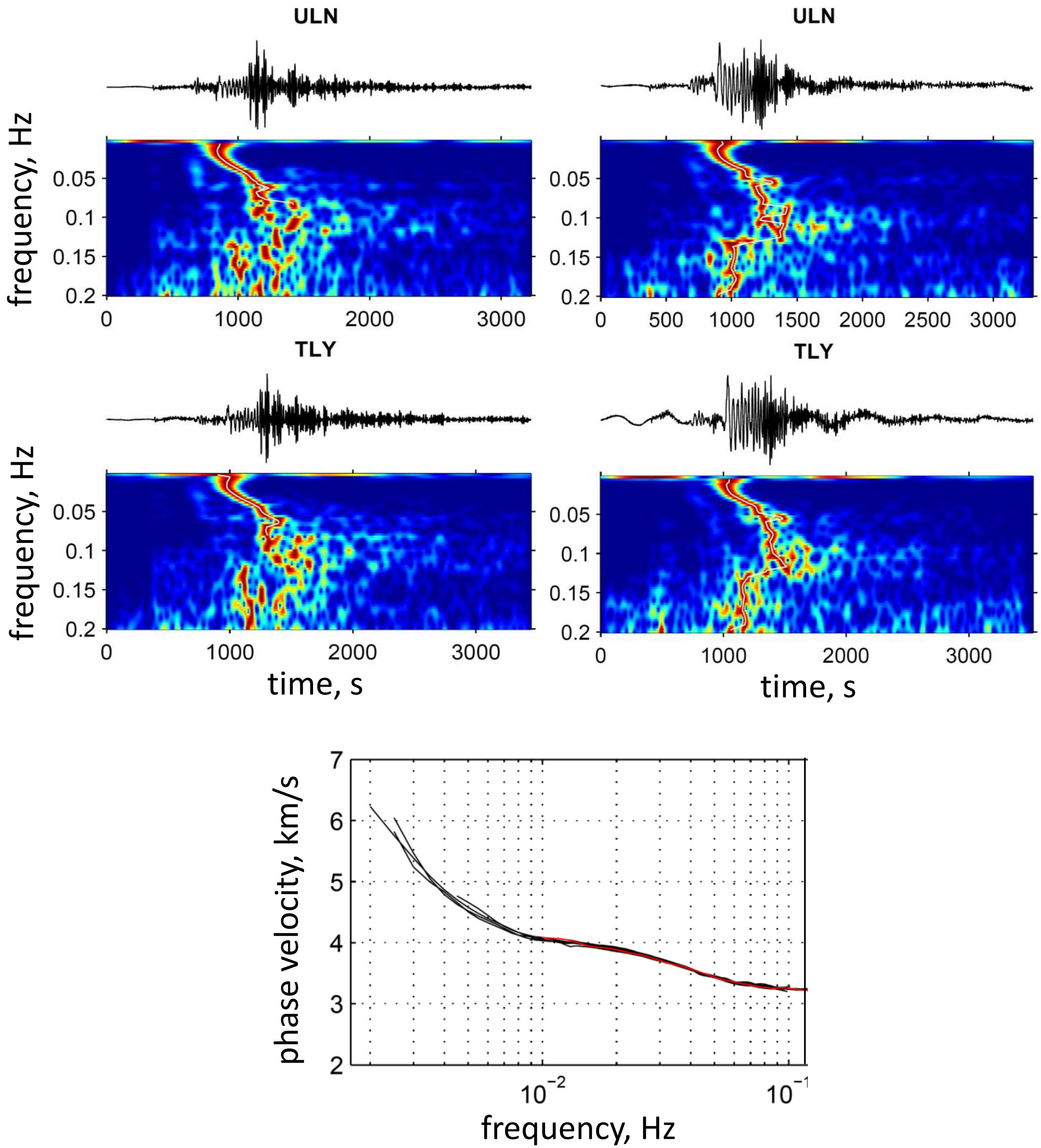
ULN
ULN
TLY
TLY
frequency, Hz
frequency, Hz
0.05
0.1
0.15
0.2
0
500
1000
1500
2000
2500
3000
time, s
time, s
phase velocity, km/s
7
6
5
4
3
2
10^{-2}
10^{-1}
frequency, Hz

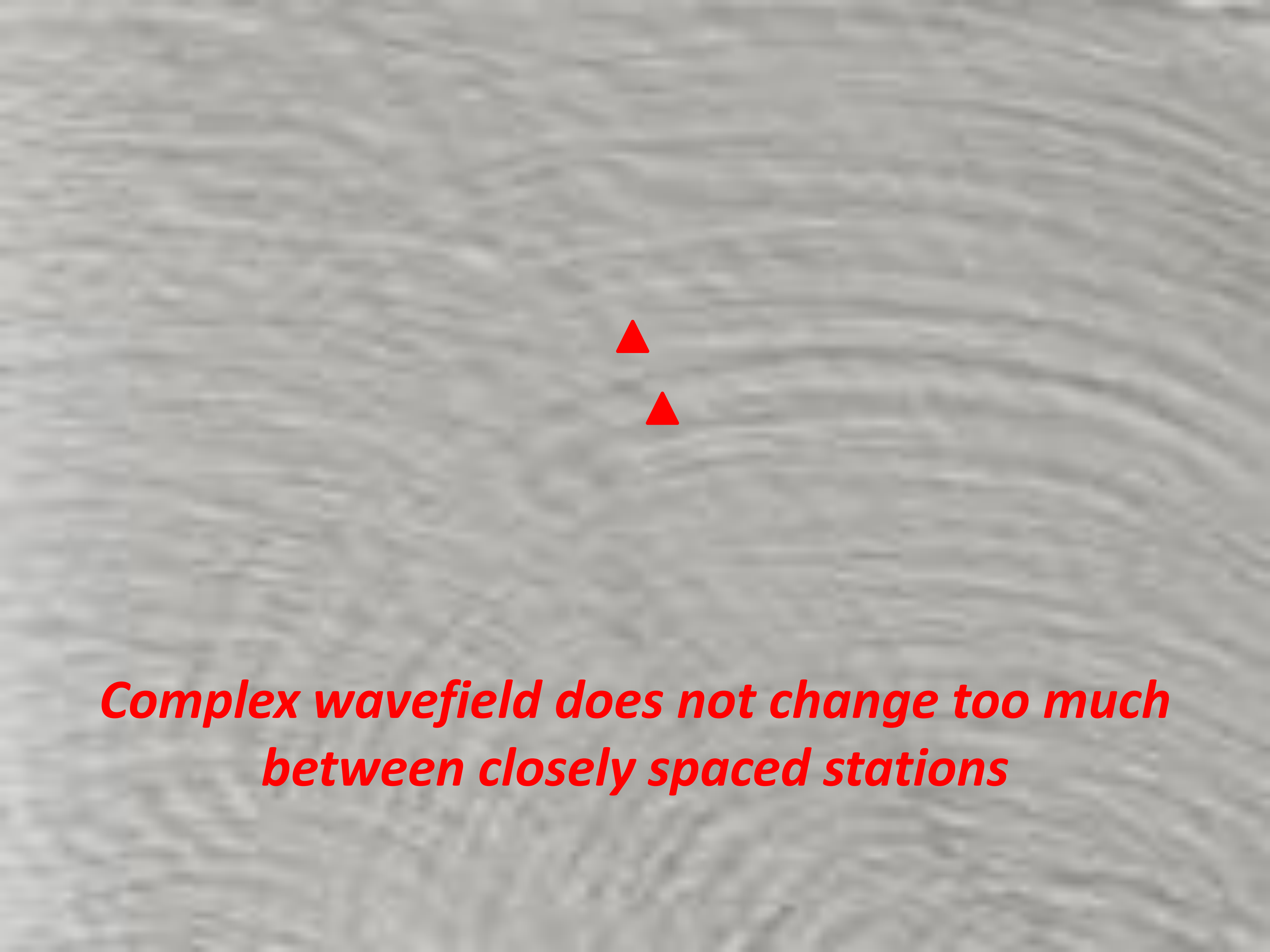

Complex wavefield does not change too much between closely spaced stations

Cross-correlation + waveform inversion: Teleseismic Interferometry

- *Cross-correlation:* applicable even to strongly diffracted surface waves, at periods down to 5 s and below
- *Waveform inversion:* The fundamental - higher mode interference taken into account, measurements up to 300-400 s periods
- Accurate measurements in very broad frequency bands (5 – 300 s)

Array imaging: The Aegean Sea

GPS measurements

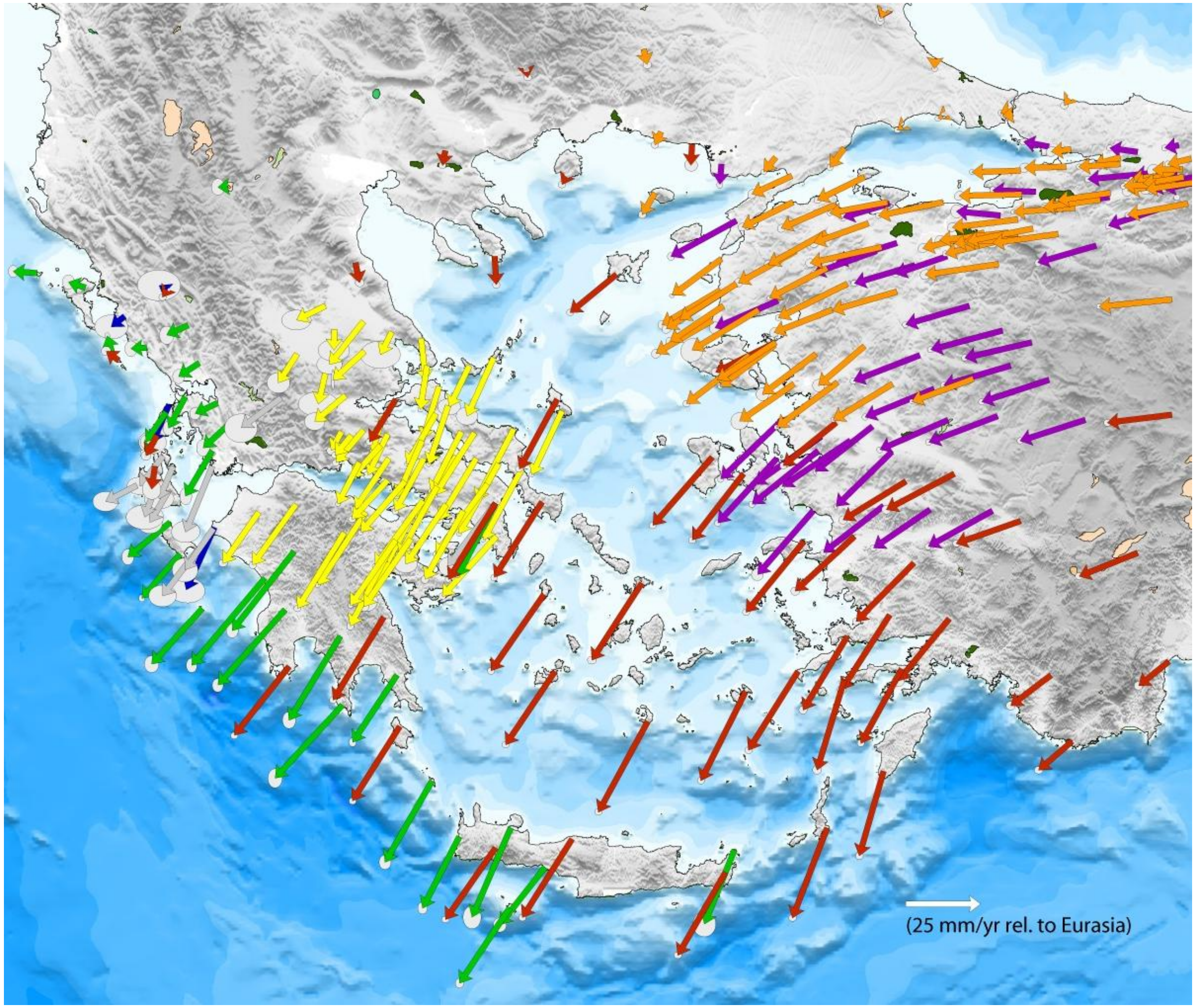

Kreemer and Chamot-Rooke 2004

Surface-wave imaging of anisotropy

- Interstation surface-wave measurements
- Anisotropic surface-wave tomography

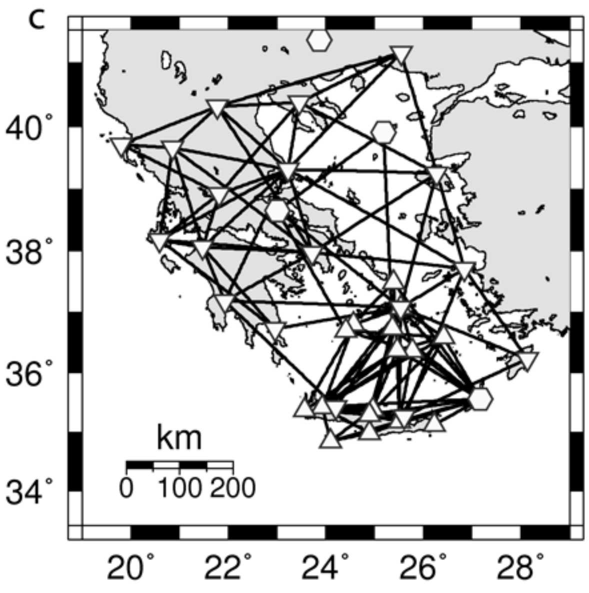

Lower crust (15-30 km depth)

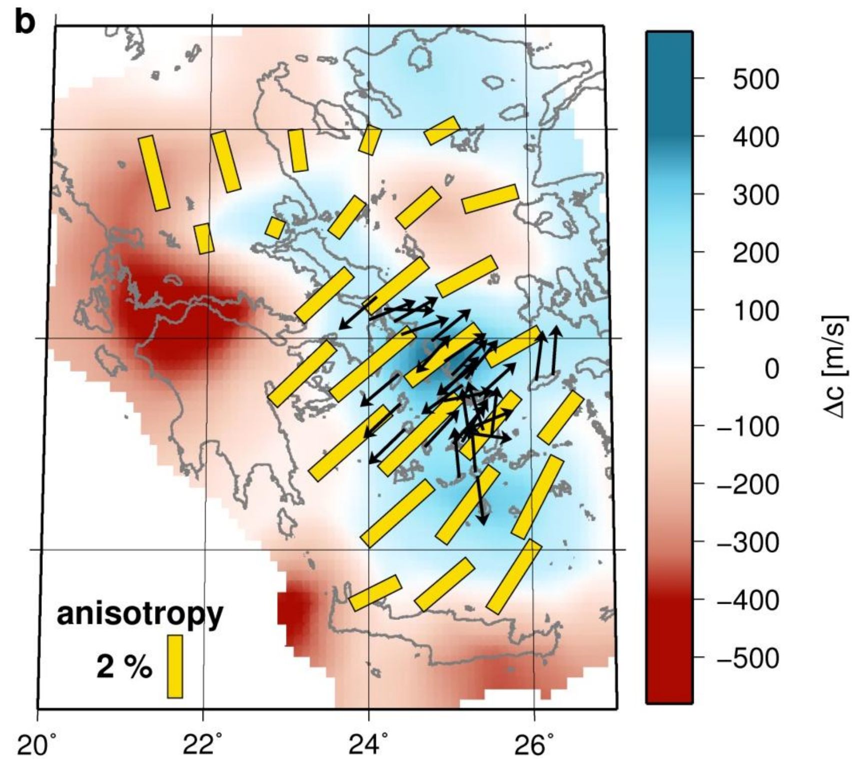

Endrun *et al.,* Nature Geo 2011

Lithospheric deformation: the Aegean

Miocene extension (> 5 Ma):

- extensional domes (core complexes) in the Cyclades
- flow in the lower crust

Stretching lineations in metamorphic core complexes

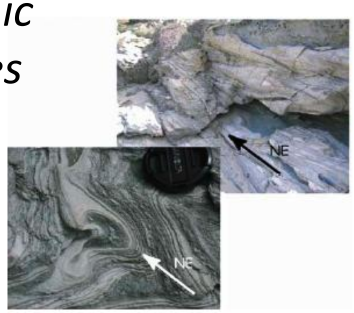

Mehl *et al* 2007

Lower crust (15-30 km depth)

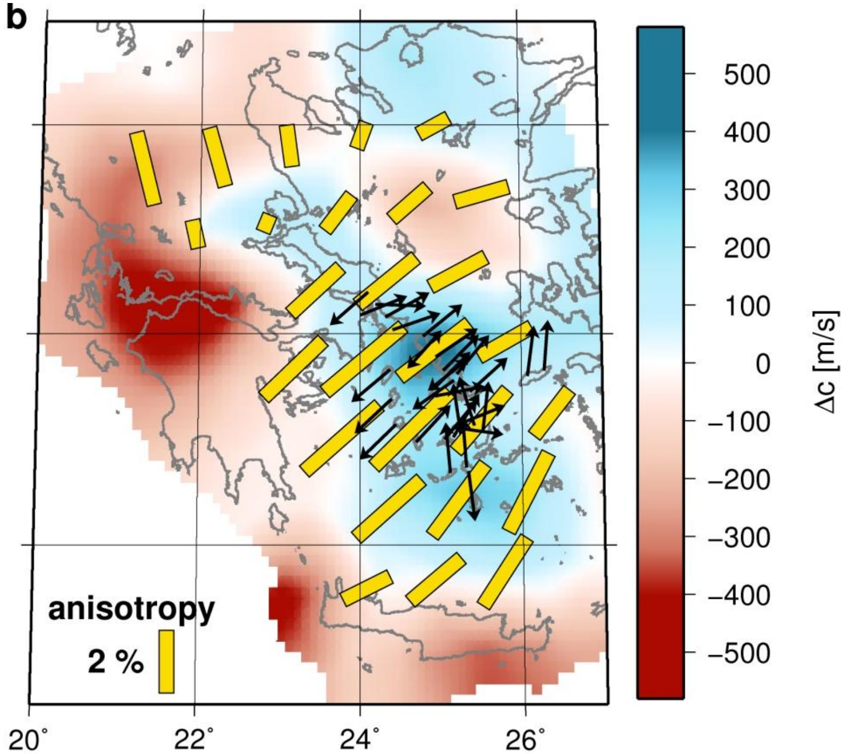

Endrun *et al.,* Nature Geo 2011

Lithospheric deformation: the Aegean

Miocene extension (> 5 Ma):

- extensional domes (core complexes) in the Cyclades
- flow in the lower crust

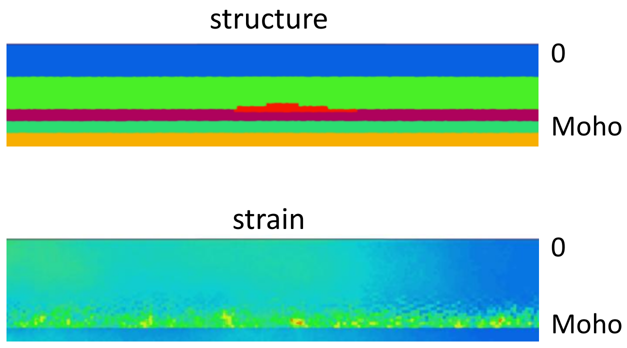

Tirel *et al.*, JGR 2008

Lower crust (15-30 km depth)

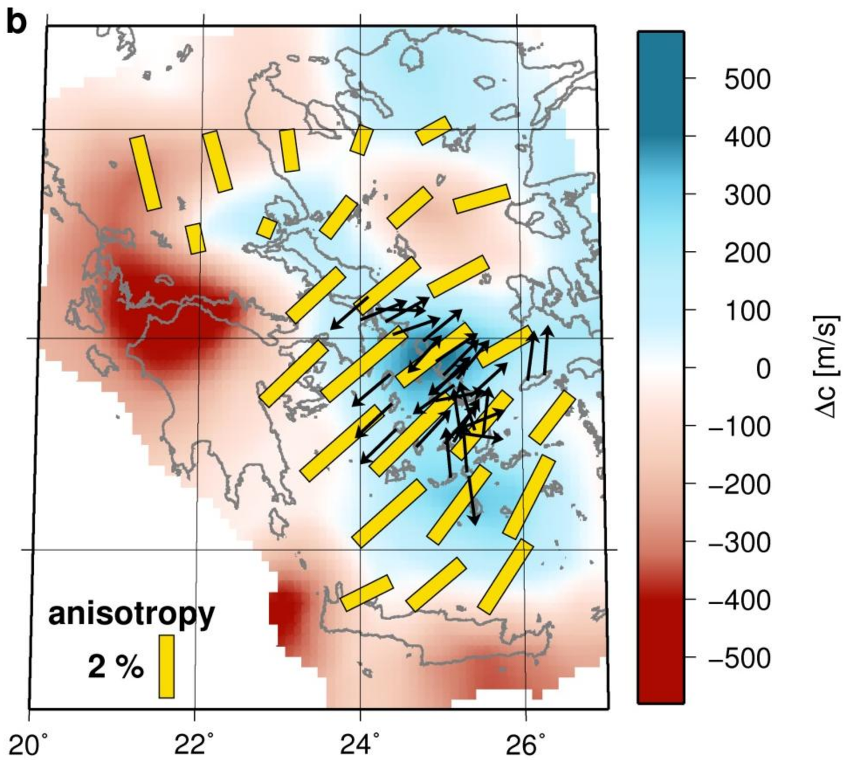

Endrun *et al.*, Nature Geo 2011

Lithospheric deformation: the Aegean

- *Anisotropy in the mantle lithosphere:*
  fast directions parallel to the extensional component
  of the strain rate field

- *North Aegean Sea:*
  N-S extension, N-S flow in the mantle lithosphere

Mantle lithosphere (30-60 km)

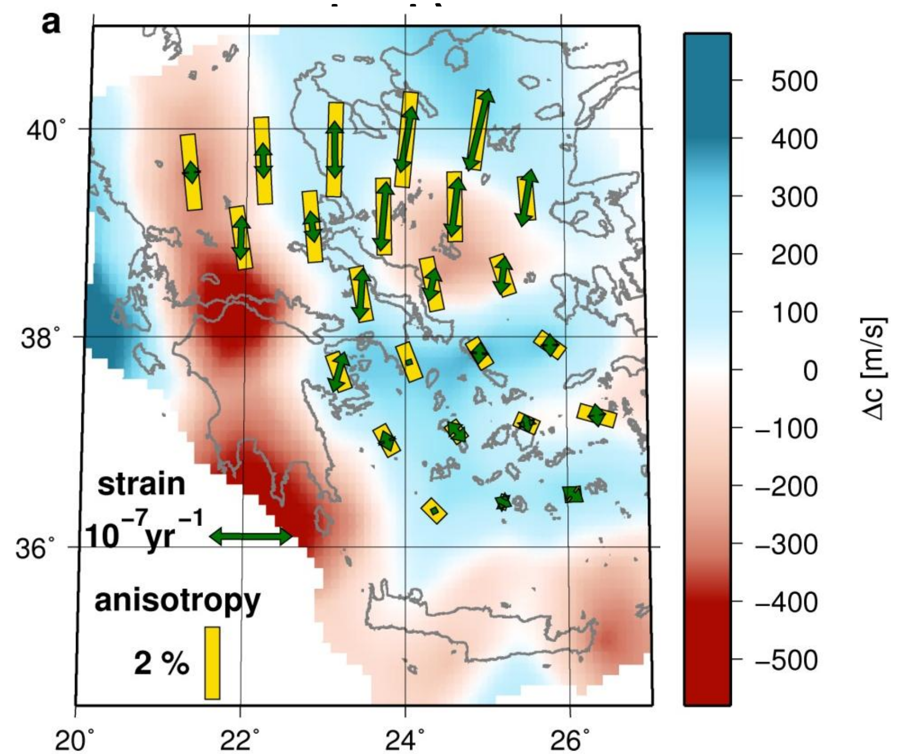

Endrun *et al.,* Nature Geo 2011

The Aegean

Grey arrows:
paleo extension (> 5 Ma), from stretching lineations.

Orange arrows:
current extension, from GPS measurements.

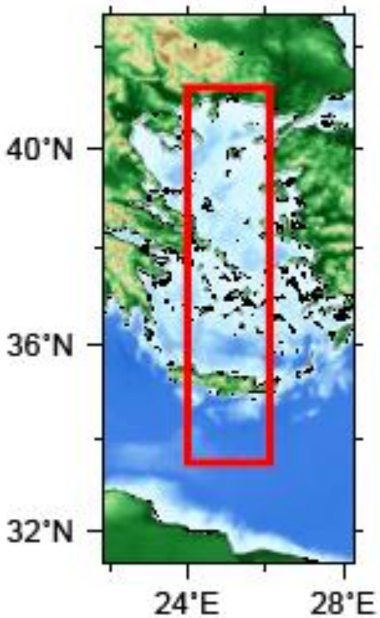

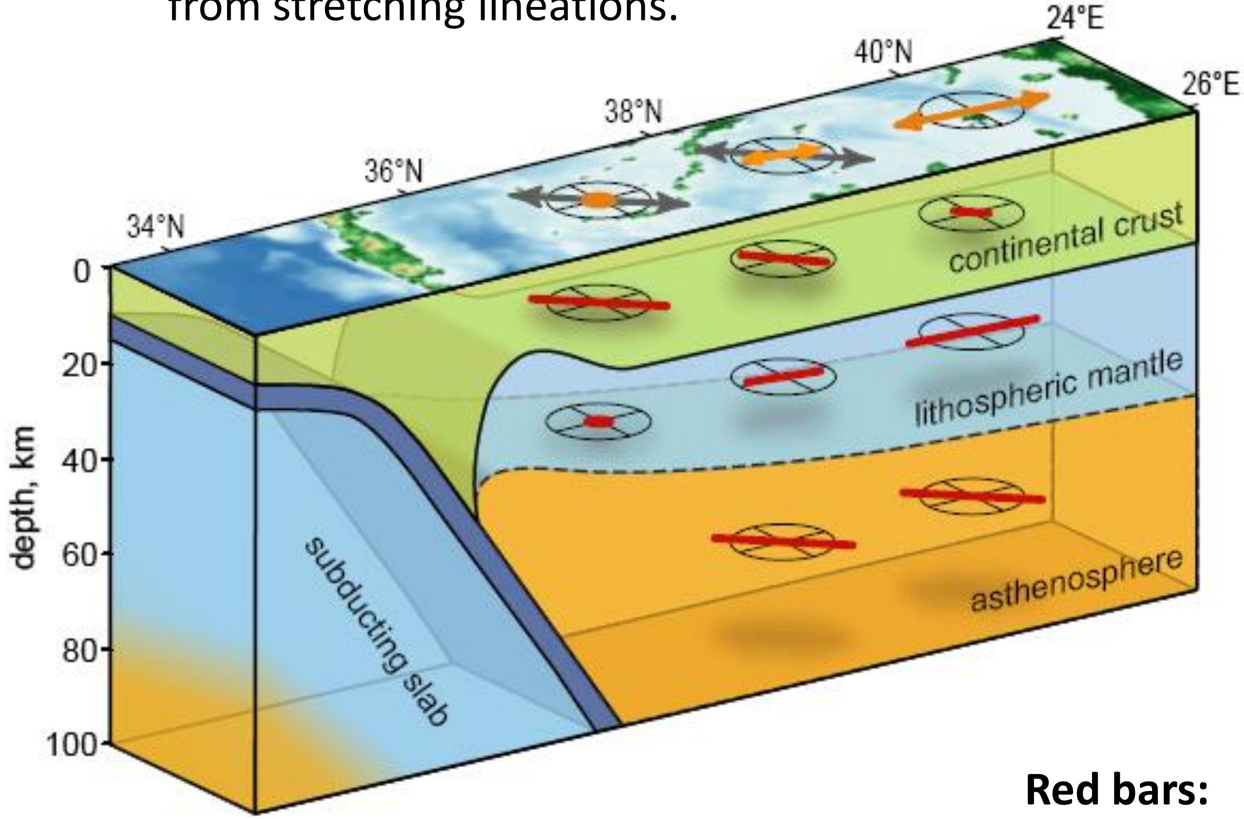

Red bars:
Anisotropic fabric at depth (current and past flow directions)

Endrun *et al.,* Nature Geo 2011

Extension mechanism in the northern Aegean Sea

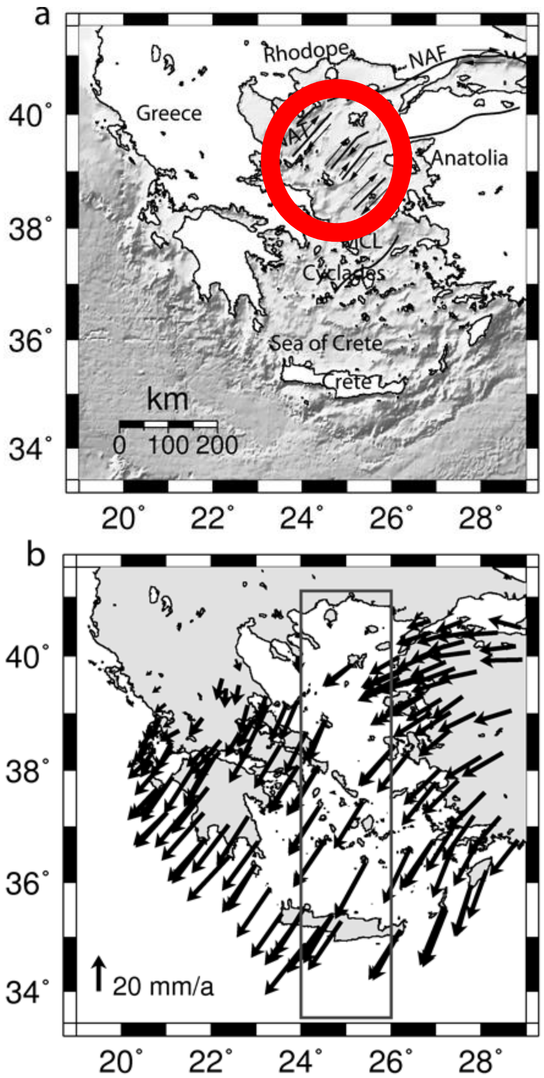

- **Upper crust:** strike-slip faulting, counter-clockwise rotation, stretching
- **Mantle lithosphere:** viscous flow North-South, parallel to the extensional component of the strain rate field
- **Lower crust:** transitional layer, with viscous flow parallel to the strike-slip faults

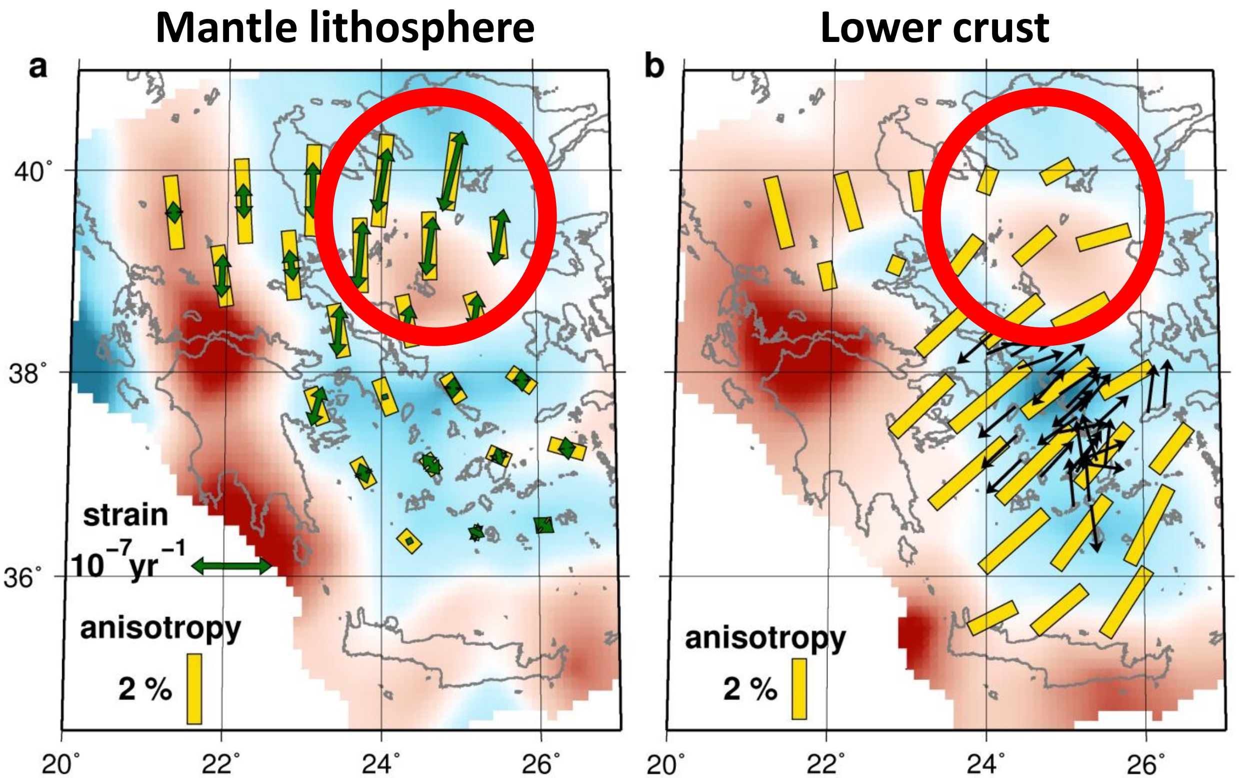

Endrun *et al.*, Nature Geo 2011

Eastern Mediterranean

- The shear associated with the westward motion of Anatolia is localised at the North Anatolian Fault, at a transition between mechanically strong (the Black Sea) and weak (Anatolia) lithospheric blocks.

Large-scale tomography

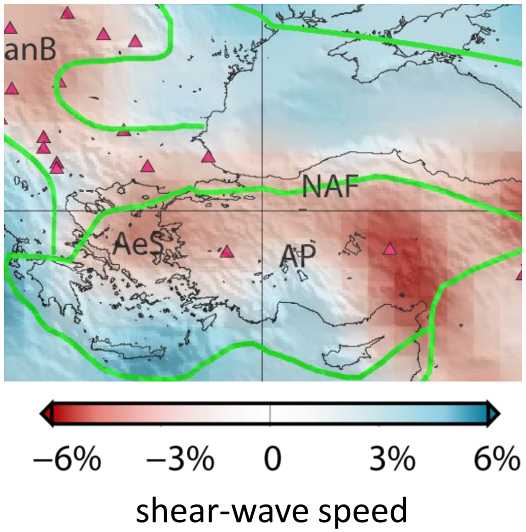

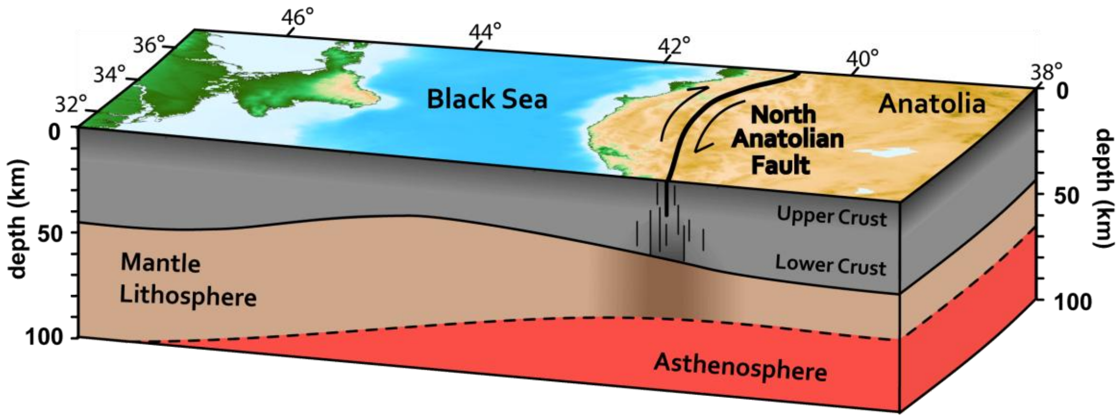

Legendre et al. 2012

Neenan et al., Lebedev et al., EGU 2012

Eastern Mediterranean

- The shear associated with the westward motion of Anatolia is localised at the North Anatolian Fault, at a transition between mechanically strong (the Black Sea) and weak (Anatolia) lithospheric blocks.

- In the warm lithosphere of northern Aegean Sea, extension is accommodated by a previously unknown mechanism: viscous flow in the mantle lithosphere that is parallel to the N-S regional extension but at an angle to the NE-SW strike-slip faults in the brittle upper crust.

III. Petro-physical inversion of surface-wave data

Composition, temperature, pressure within the lithosphere

Thermodynamic calculation for an equilibrium mineral assemblage

PERPLEX (J. Connoly)
LITMOD (J. Fullea et al.)

Density, elastic parameters

Calculation of phase velocities for 1-D Earth models

Normal-mode code (e.g., MINEOS)

Surface-wave observables

Fullea, Lebedev, Agius, Jones, Afonso, 2012

Petro-physical inversion of surface-wave data

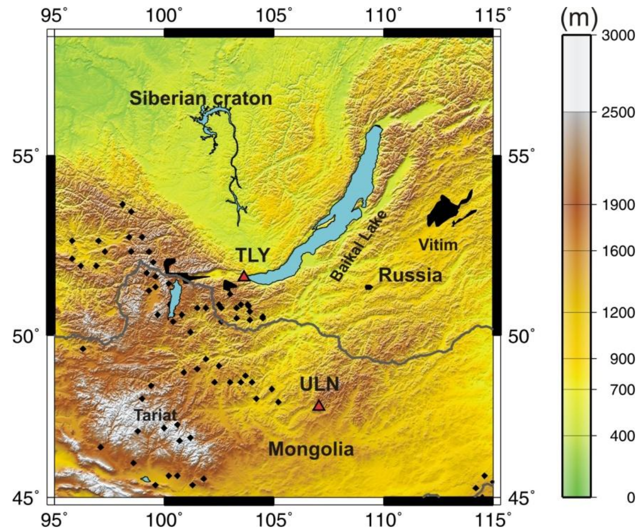

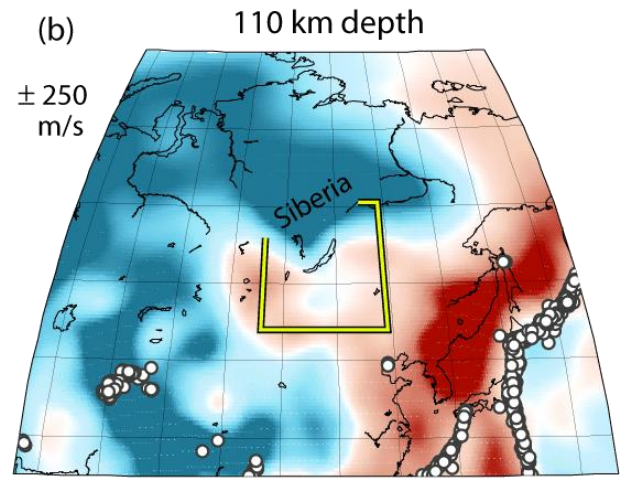

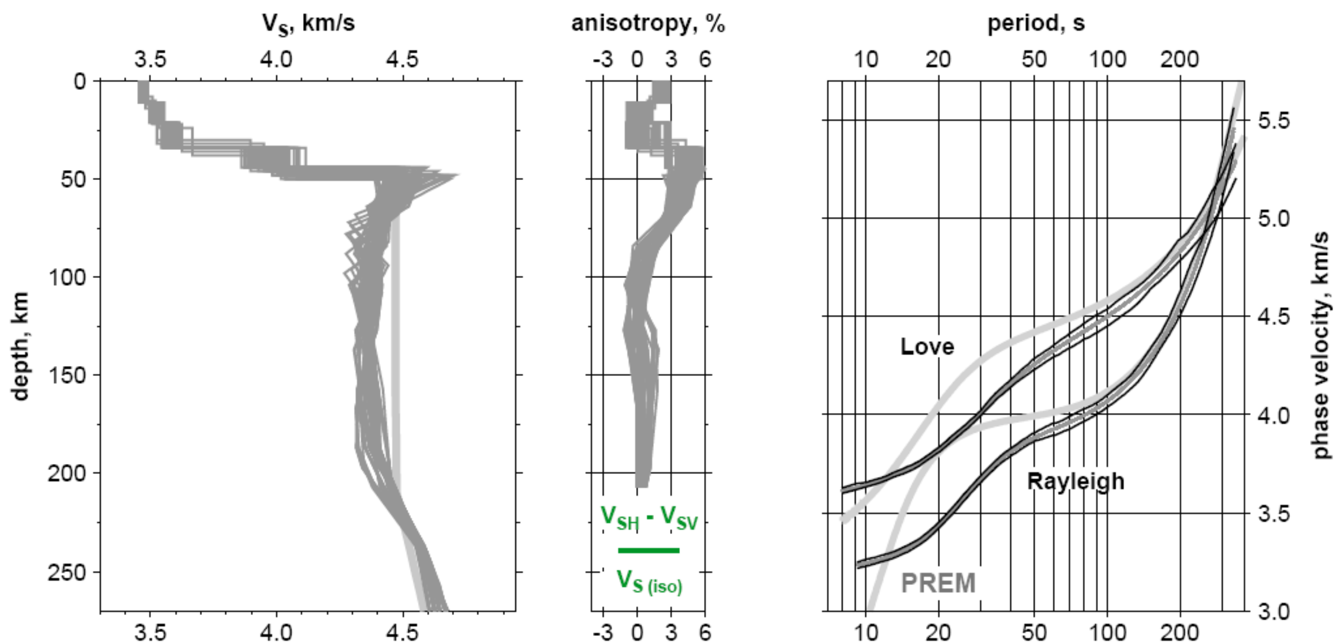

Petro-physical inversion of surface-wave data

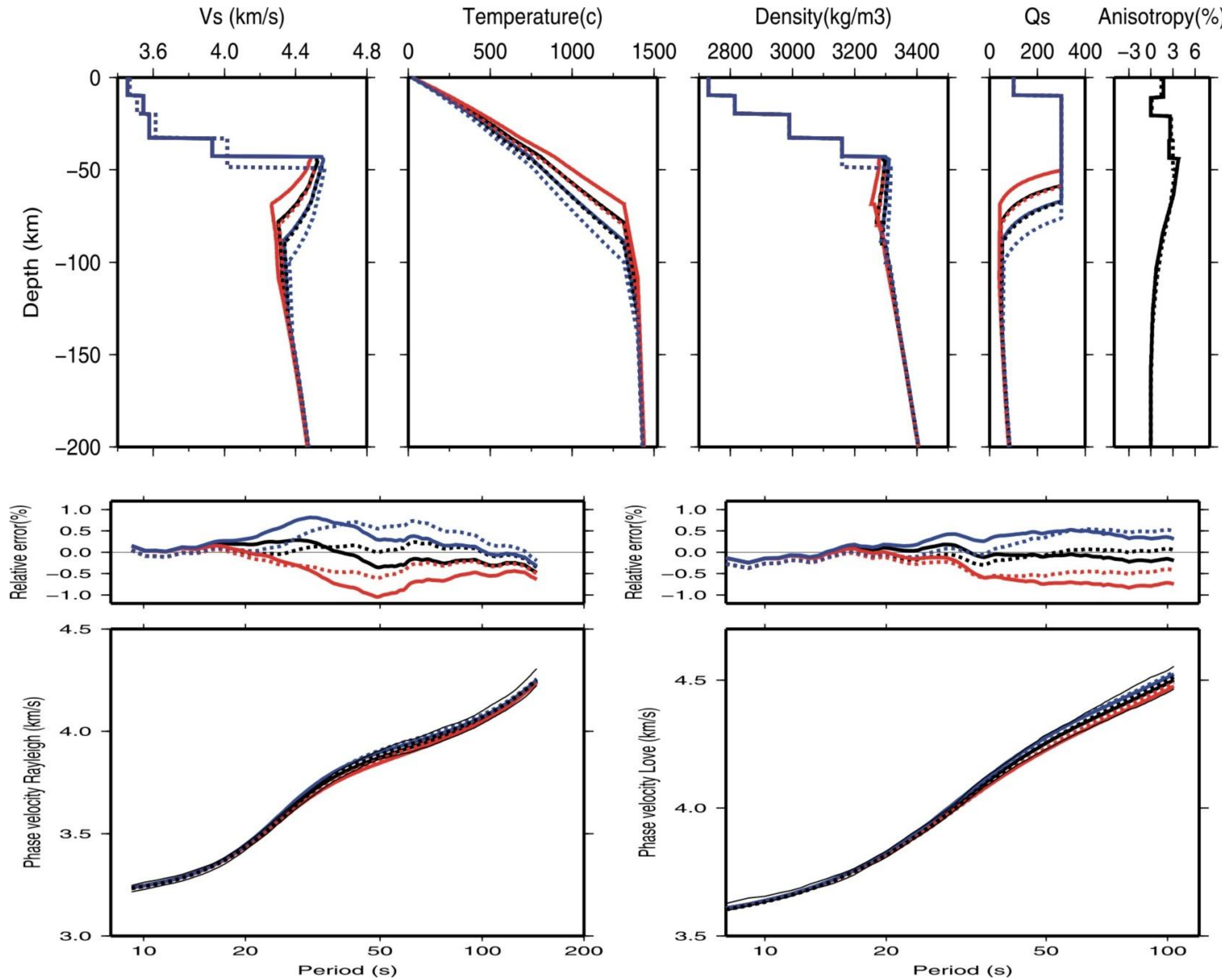

Fullea, Lebedev, Agius, Jones, Afonso, 2012

Petro-physical inversion of surface-wave data

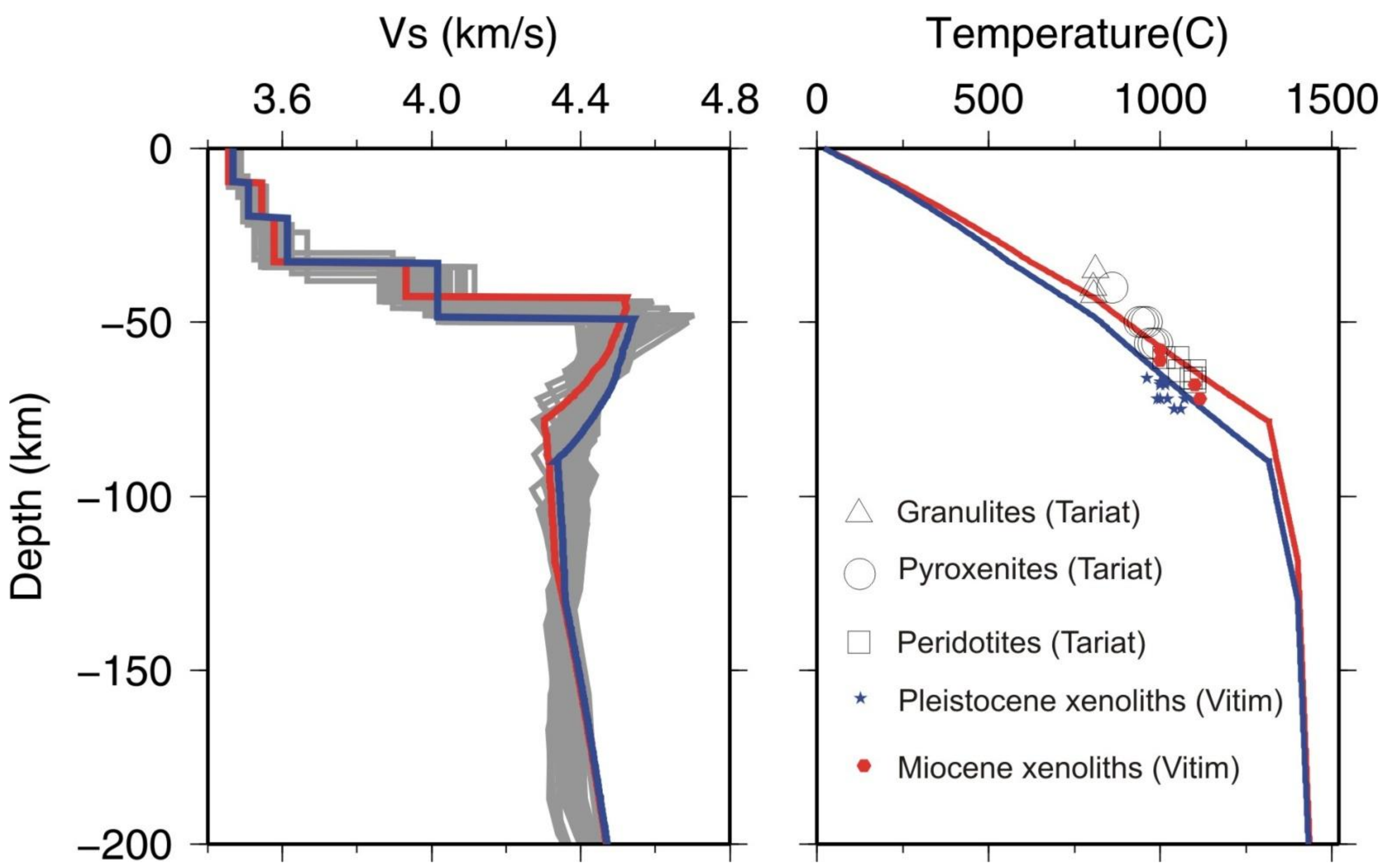

Fullea, Lebedev, Agius, Jones, Afonso, 2012

Ireland Array

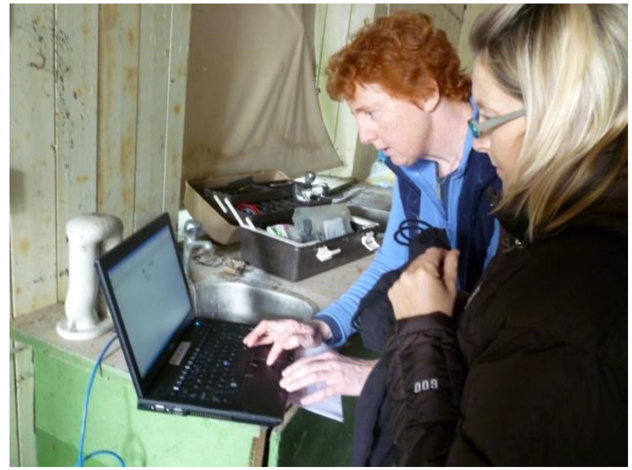

Ireland Array

2010-2012: deployment of the backbone component, for 5 years. 20 broad-band stations (Trillium 120)

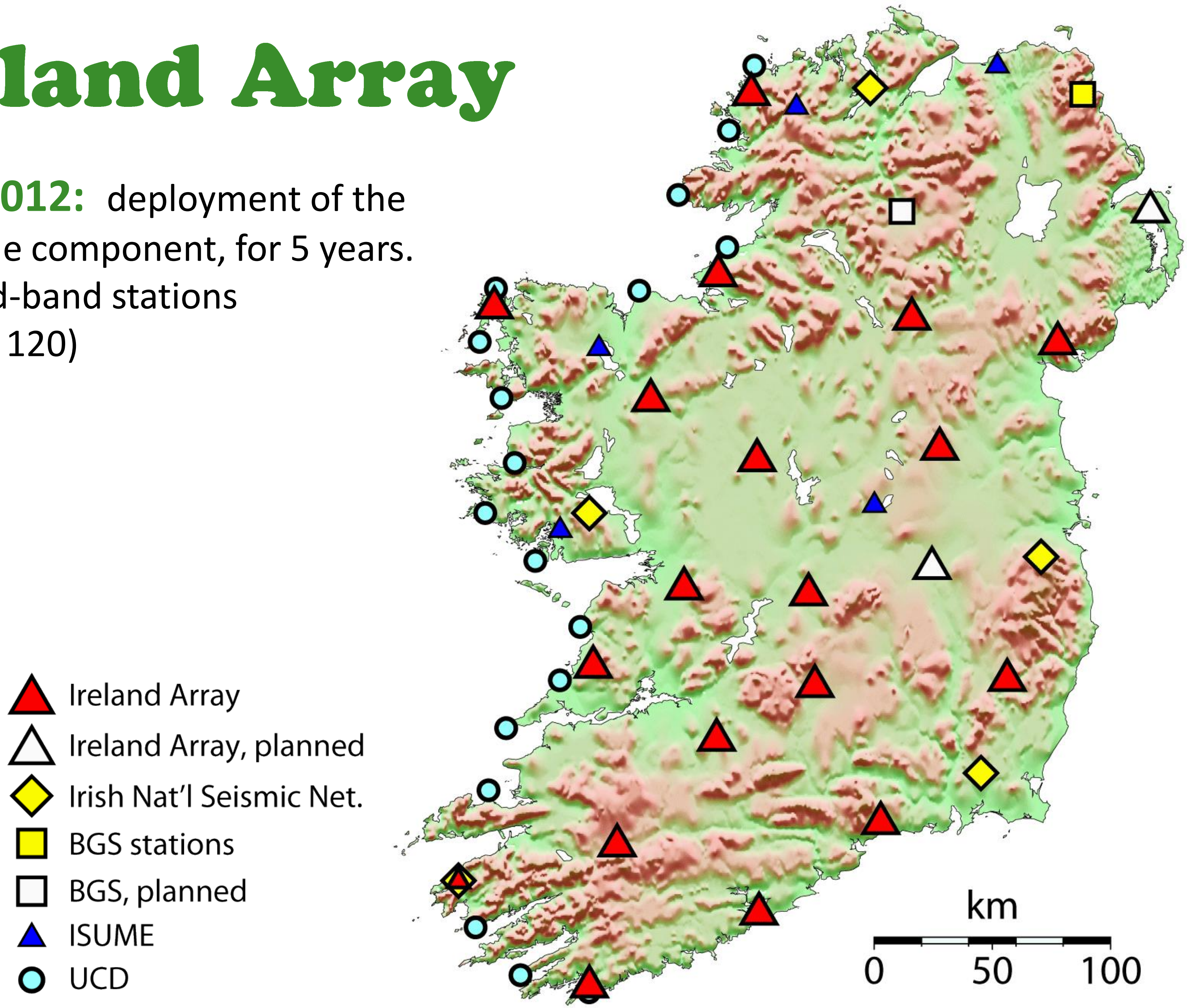

Ireland Array station IA002, Co. Sligo

Ireland Array: seismograms

Earthquake Magnitude: 7.5
Location: Indonesia, Kepulauan Mentawai region
Date and Time: 2010/10/25 14:42:25.00
Latitude: 3.100 S, Longtitude: 100.200 E, Depth: 33.0
Recorded at: Ireland Array station IAVAL, Co. Kerry

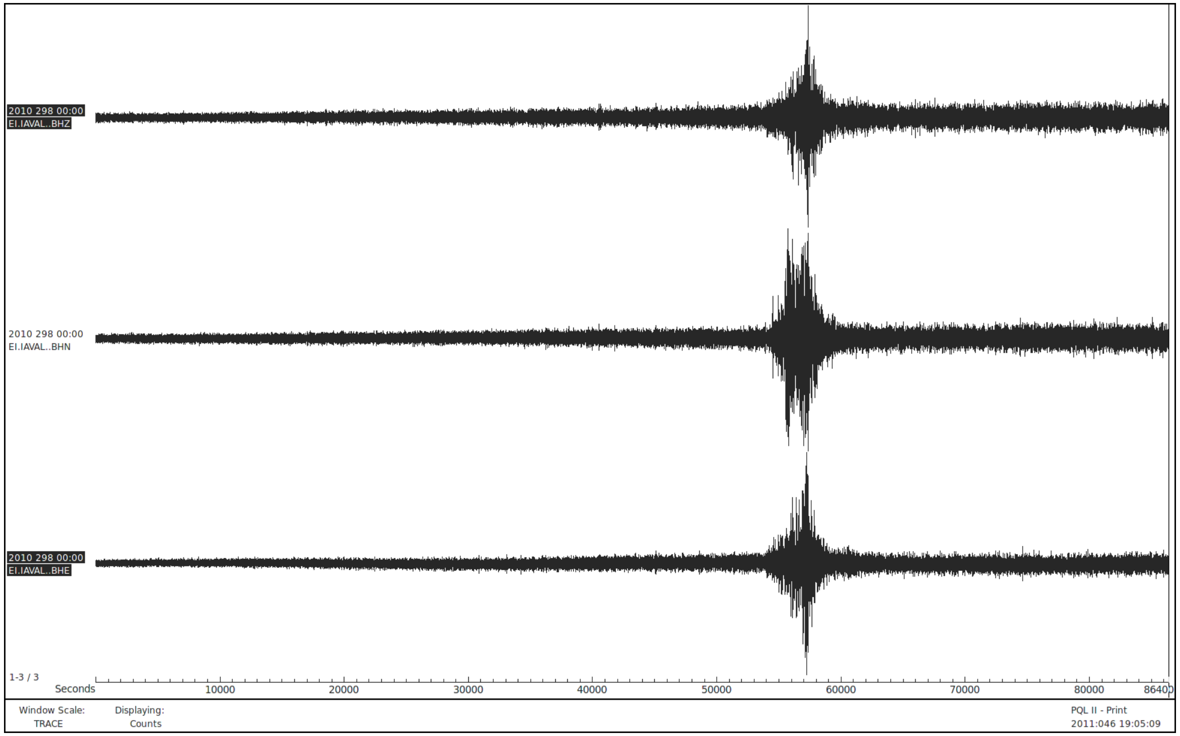

SIM-CRUST

Seismic Imaging and Monitoring of Ireland's Crust for geothermal resource assessment

- Seismic-velocity model of Ireland's crust
- Monitoring of seismicity and analysis of tectonic stress and secondary porosity using dense arrays
- 4D tomography

Funded by Science Foundation Ireland SIRG grant (550K total)
N. Piana Agostinetti, A. Licciardi, S. Lebedev

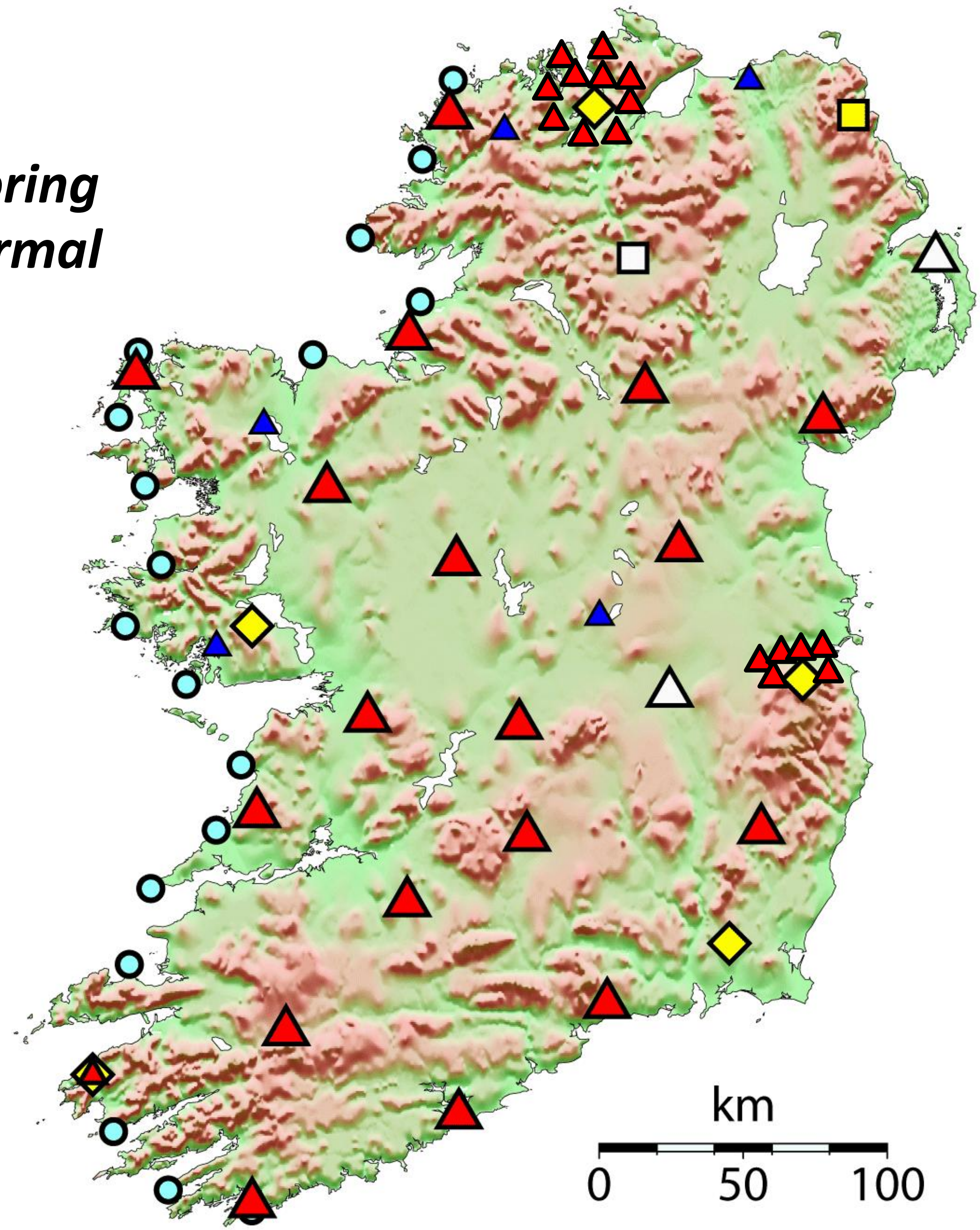

Thermal structure of Ireland's lithosphere and geothermal resource assessment

Temperature at 2.5 km | Heat Flow Density

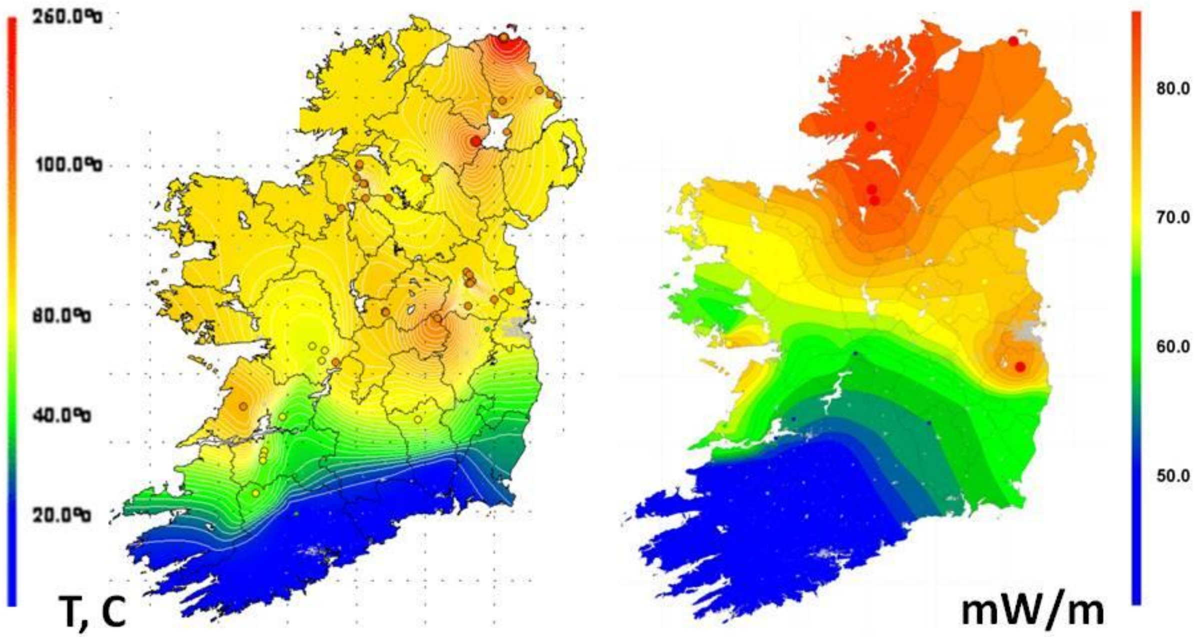

after Goodman et al. 2004

Thermal structure of Ireland's lithosphere and geothermal resource assessment

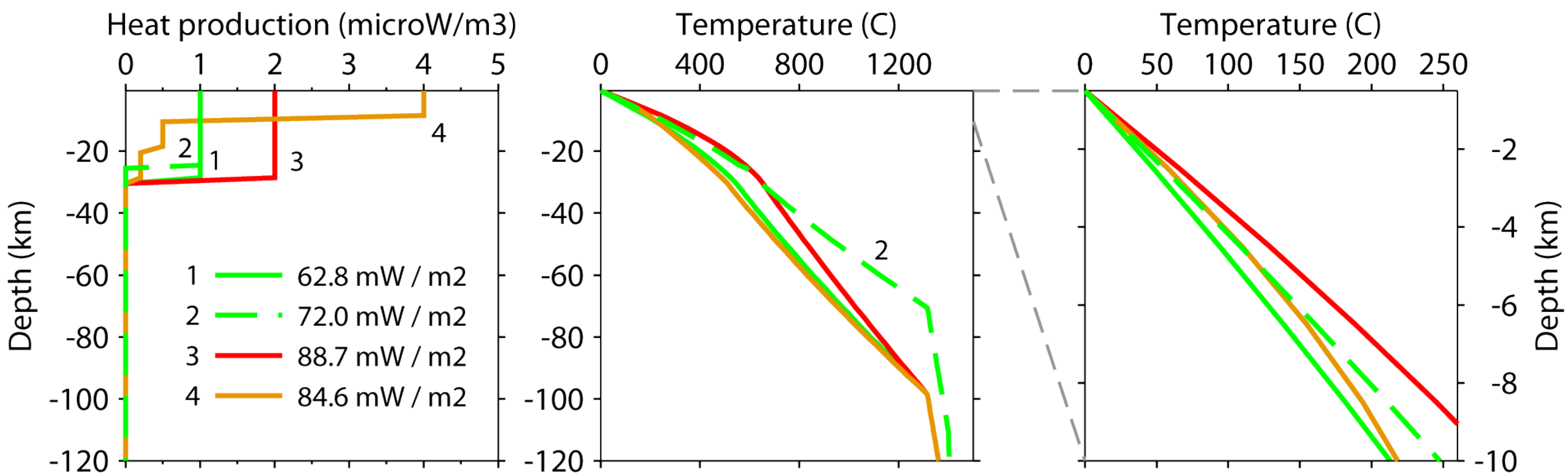

- 4 geotherms: different lithospheric thicknesses and crustal heat productions
- all can fit topography and the heat flow measured in Ireland
- a lithospheric thickness change from 100 to 70 km will increase the temperature at 4-5 km depth by 20C, and heatflow by 10 mW/m2
- deep thermal structure of the lithosphere will be determined by petro-physical inversions of Ireland Array seismic data

Summary: regional and global tomography

- waveform tomography ⟶
  lateral variations in the thermal structure and dynamics of the lithosphere and upper mantle

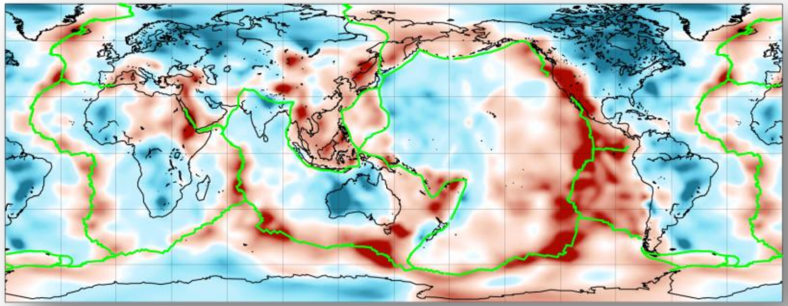

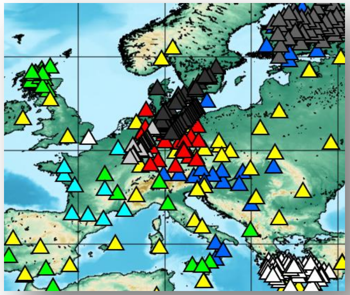

- dense arrays of station ⟶
  high-resolution regional structure and anisotropy, lithospheric dynamics

- petrophysical inversion of surface-wave data ⟶
  thickness, temperature and composition of the lithosphere

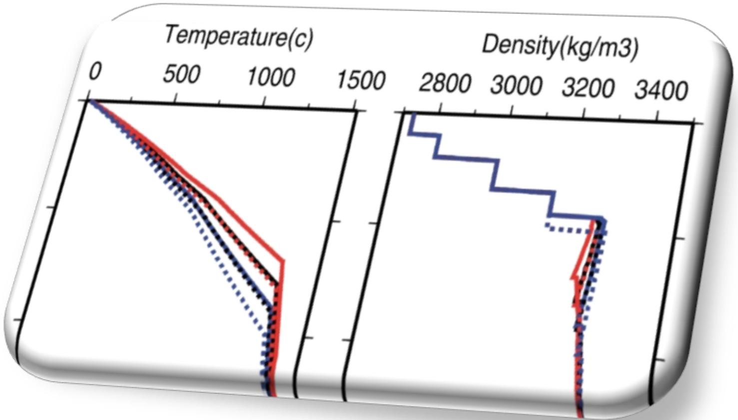

Outlook

- major improvements in the accuracy and resolution of seismic models of the Earth

- advances in petro-physical and geodynamic modelling

- multi-disciplinary, integrated inversions can now be developed, targeting fundamental mechanisms of lithospheric dynamics.